
Natural Posterior Network: Deep Bayesian Predictive Uncertainty for Exponential Family Distributions

Bertrand Charpentier,* Oliver Borchert,* Daniel Zügner, Simon Geisler, Stephan Günnemann

Technical University of Munich, Germany

{charpent, borcher, zuegnerd, geisler, guennemann}@in.tum.de

Abstract

Uncertainty awareness is crucial to develop reliable machine learning models. In this work, we propose the Natural Posterior Network (NatPN) for fast and high-quality uncertainty estimation for any task where the target distribution belongs to the exponential family. Thus, NatPN finds application for both classification and general regression settings. Unlike many previous approaches, NatPN does not require out-of-distribution (OOD) data at training time. Instead, it leverages Normalizing Flows to fit a single density on a learned low-dimensional and task-dependent latent space. For any input sample, NatPN uses the predicted likelihood to perform a Bayesian update over the target distribution. Theoretically, NatPN assigns high uncertainty far away from training data. Empirically, our extensive experiments on calibration and OOD detection show that NatPN delivers highly competitive performance for classification, regression and count prediction tasks.

1 Introduction

The *Dunning-Kruger effect* [35] describes a psychological cognitive bias in which people lacking knowledge in a particular domain overestimate their abilities. Interestingly, this phenomenon also applies to machine learning models. Traditional neural networks show overconfident predictions, in particular on data that is different from the data seen during training [28, 37]. The illusion of knowledge caused by this *Machine Learning Dunning-Kruger effect* highly impacts the reliability of such models in safety-critical domains [48]. Accurate uncertainty estimation is considered an appropriate solution to this problem, giving systems the ability to flag predictions with low confidence [59]. More specifically, a reliable model should distinguish between *aleatoric* and *epistemic* uncertainty [21]. These two levels of uncertainty allow a model to account for both irreducible data uncertainty (e.g. a fair dice’s chance of 1/6 for each face) and uncertainty due to the lack of knowledge about unseen data (e.g. input features differing significantly from training data or a covariate shift). These two aleatoric and epistemic uncertainty levels can eventually be combined into an overall *predictive uncertainty* [21].

Related Work. Generally, we distinguish between two families of models for uncertainty estimation. A first family of models estimates uncertainty by aggregating statistics (e.g. mean and variance) from different samples of an implicit predictive distribution. Examples are ensemble [37, 69, 70, 32, 68] and dropout [22] models which provide high-quality uncertainty estimates [59] at the cost of an expensive sampling phase at inference time. Moreover, ensembles usually require training multiple models. Similarly, Bayesian neural networks (BNN) [6, 62, 42] model the uncertainty on the weights. Hence, they also require multiple samples to estimate the uncertainty on the final prediction. While recent BNNs have shown reasonably good practical performances [16, 19, 58], modelling the distribution on the weights can make them less viable for complex tasks [20] causing many BNN to be limited to simple architectures [27].

*Equal contribution

In contrast, a second family of models is capable of estimating uncertainty in a single pass [38, 36]. In particular, an important model family directly predicts the parameters of a conjugate prior on the predicted target probability distribution, thus accounting for the different levels of uncertainty. Most of those models focus on classification and thus predict parameters of a Dirichlet distribution [44, 45, 9, 3, 53, 67, 78, 65]. So far, only two works [1, 43] have tried to learn a Normal Inverse-Gamma (NIG) distribution as a prior for regression. However, all these models are limited to a single task (e.g. either classification or regression). Some approaches even require out-of-distribution (OOD) data at training time [44, 45] which is an unrealistic assumption in most applications where anomalies are a priori rare or unknown.

Our Contribution. We propose Natural Posterior Network (NatPN) a new simple, flexible and sound approach for fast and high quality uncertainty predictions. **(Simple)** NatPN only adds a single normalizing flow density to the last predictor layer and does not need OOD data for training. **(Flexible)** NatPN can estimates predictive uncertainty for *any* tasks described by the general group of exponential family distributions. Notably, this encompasses very common tasks such as classification, regression and count prediction which can be described with Categorical, Normal and Poisson distributions, respectively. **(Sound)** NatPN is based on a new unified exponential family framework which performs an input-dependent Bayesian update. For every input, it predicts the parameters of the posterior over the target exponential family distribution. We show that this Bayesian update is guaranteed to predict high uncertainty far from training data. **(Fast)** NatPN provides fast uncertainty estimation in a single forward pass with a single normalizing flow. **(High Quality)** Our extensive experiments showcase the high performances of NatPN for various criteria (accuracy, calibration, OOD and shift detection) and tasks (classification, regression and count prediction). We illustrate the accurate aleatoric and predictive uncertainty predictions of NatPN on two toy examples for classification and regression in Fig. 1. *None of the related works* have similar properties.

2 Natural Posterior Network

At the very core of NatPN stands the Bayesian update rule: $\mathbb{Q}(\boldsymbol{\theta} | \mathcal{D}) \propto \mathbb{P}(\mathcal{D} | \boldsymbol{\theta}) \times \mathbb{Q}(\boldsymbol{\theta})$ where $\mathbb{P}(\mathcal{D} | \boldsymbol{\theta})$ is the target distribution of the target data \mathcal{D} given its parameter $\boldsymbol{\theta}$, and $\mathbb{Q}(\boldsymbol{\theta})$ and $\mathbb{Q}(\boldsymbol{\theta} | \mathcal{D})$ are the prior and posterior distributions, respectively, over the target distribution parameters. The target distribution $\mathbb{P}(\mathcal{D} | \boldsymbol{\theta})$ could be any likelihood describing the observed target labels. The Bayesian update has three main advantages: **(1)** it introduces a prior belief which represents the safe default prediction if no data is observed, **(2)** it updates the prior prediction based on observed target labels, and **(3)** it assigns a confidence for the new target prediction given the aggregated evidence count of observed target labels. While NatPN is capable to perform a Bayesian update for every possible input given the observed training data, we first recall the Bayesian background for a single exponential family distribution.

Likelihood \mathbb{P}	Conjugate Prior \mathbb{Q}	Parametrization Mapping m	Bayesian Loss (Eq. 5)
$y \sim \text{Cat}(\boldsymbol{p})$	$\boldsymbol{p} \sim \text{Dir}(\boldsymbol{\alpha})$	$\chi = \boldsymbol{\alpha}/n$ $n = \sum_c \alpha_c$	(1) = $\psi(\alpha_{y*}^{(i)}) - \psi(\alpha_0^{(i)})$ (2) = $\log B(\boldsymbol{\alpha}^{(i)}) + (\alpha_0^{(i)} - C)\psi(\alpha_0^{(i)}) - \sum_c (\alpha_c^{(i)} - 1)\psi(\alpha_c^{(i)})$
$y \sim \mathcal{N}(\mu, \sigma)$	$\mu, \sigma \sim \mathcal{N}^{-1}(\mu_0, \lambda, \alpha, \beta)$	$\chi = \begin{pmatrix} \mu_0 \\ \mu_0 + \frac{2\beta}{n} \end{pmatrix}$ $n = \lambda = 2\alpha$	(1) = $\frac{1}{2} \left(-\frac{\alpha}{\beta}(y - \mu_0)^2 - \frac{1}{\lambda} + \psi(\alpha) - \log \beta - \log 2\pi \right)$ (2) = $\frac{1}{2} + \log \left((2\pi)^{\frac{1}{2}} \beta^{\frac{3}{2}} \Gamma(\alpha) \right) - \frac{1}{2} \log \lambda + \alpha - (\alpha + \frac{3}{2})\psi(\alpha)$
$y \sim \text{Poi}(\lambda)$	$\lambda \sim \Gamma(\alpha, \beta)$	$\chi = \alpha/n$ $n = \beta$	(1) = $(\psi(\alpha) - \log \beta)y - \frac{\alpha}{\beta} - \sum_{k=1}^y \log k$ (2) = $\alpha + \log \Gamma(\alpha) - \log \beta + (1 - \alpha)\psi(\alpha)$

Table 1: Examples of Exponential Family Distributions where $\psi(x)$ and $B(x)$ denote Digamma and Beta function, respectively.

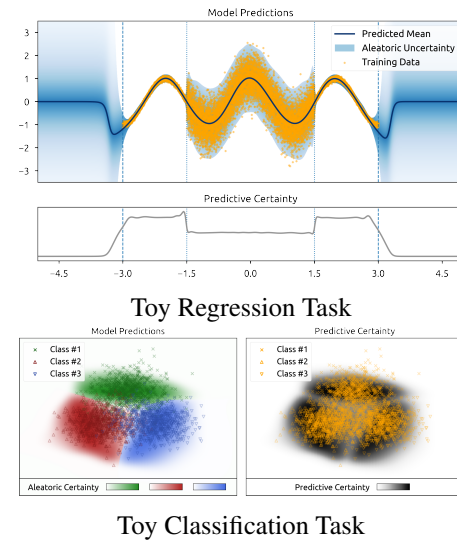


Figure 1: Visualization of the aleatoric and predictive uncertainty estimates of NatPN on two toy regressions and classification tasks. NatPN correctly assigns higher uncertainty to regions far from the training data.

Exponential Family Distribution. Distributions from the exponential family are very widely used and have favorable analytical properties. Indeed, **(1)** they cover a wide range of target variables like discrete, continuous, counts or spherical coordinates, and **(2)** they benefit from intuitive and generic formulae for their parameters, density functions and statistics which can often be evaluated in closed-form. Important examples of exponential family distributions are Normal, Categorical and Poisson distributions (see Tab. 1). Formally, an exponential family distribution on a target variable $y \in \mathbb{R}$ with *natural parameters* $\theta \in \mathbb{R}^L$ can be denoted as

$$\mathbb{P}(y | \theta) = h(y) \exp(\theta^T \mathbf{u}(y) - A(\theta)) \quad (1)$$

where $h : \mathbb{R} \rightarrow \mathbb{R}$ is the *carrier or base measure*, $A : \mathbb{R}^L \rightarrow \mathbb{R}$ the *log-normalizer* and $\mathbf{u} : \mathbb{R} \rightarrow \mathbb{R}^L$ the *sufficient statistics* [57, 4]. The entropy of an exponential family distribution can always be written as $\mathbb{H}[\mathbb{P}] = A(\theta) - \theta^T \nabla_{\theta} A(\theta) - \mathbb{E}[\log h(y)]$ [57]. An exponential family distribution always admits a conjugate prior, which often also is a member of the exponential family:

$$\mathbb{Q}(\theta | \chi, n) = \eta(\chi, n) \exp(n \theta^T \chi - n A(\theta)) \quad (2)$$

where $\eta(\chi, n)$ is a normalization coefficient, $\chi \in \mathbb{R}^L$ are *prior parameters* and $n \in \mathbb{R}^+$ is the *evidence*. Given a set of N target observations $\{y^{(i)}\}_i^N$, it is easy to compute a closed-form Bayesian update $\mathbb{Q}(\theta | \chi^{\text{post}}, n^{\text{post}}) \propto \mathbb{P}(\{y^{(i)}\}_i^N | \theta) \times \mathbb{Q}(\theta | \chi^{\text{prior}}, n^{\text{prior}})$:

$$\mathbb{Q}(\theta | \chi^{\text{post}}, n^{\text{post}}) \propto \exp(n^{\text{post}} \theta^T \chi^{\text{post}} - n^{\text{post}} A(\theta)) \quad (3)$$

where $\chi^{\text{post}} = \frac{n^{\text{prior}} \chi^{\text{prior}} + \sum_j^N \mathbf{u}(y^{(j)})}{n^{\text{prior}} + N}$ and $n^{\text{post}} = n^{\text{prior}} + N$. We see that χ^{prior} (resp. χ^{post}) can be viewed as the average sufficient statistics of n^{prior} (resp. n^{post}) fictitious samples [4]. Further the average sufficient statistic of the fictitious samples is equal to the average sufficient statistic of the conjugate distribution i.e. $\chi = \mathbb{E}_{\mathbb{Q}(\chi, n)}[\theta]$ [7, 13]. Therefore, the parameter χ^{post} carries the inherent aleatoric uncertainty on the target distribution with natural parameters θ , while the evidence n^{post} aligns well with the epistemic uncertainty (i.e. a low evidence means few prior target observations). We emphasize that the natural conjugate prior parametrization χ, n is often different from the “well known” parametrization κ . By definition, a bijective mapping $m(\kappa) = (\chi, n)$ from the natural parametrization to the commonly used parametrization always exists (see examples in Tab. 1). Finally, exponential family distributions always admit a closed-form predictive posterior distribution [24].

Input-Dependent Bayesian Update for Exponential Family Distributions. We propose to leverage the power of exponential family distributions for the more complex task when the prediction $y^{(i)}$ depends on the input $\mathbf{x}^{(i)}$. Hence, NatPN extends the Bayesian treatment of a single exponential family distribution prediction by predicting an individual posterior update per input. We distinguish between the chosen prior parameters $\chi^{\text{prior}}, n^{\text{prior}}$ shared among samples, and the additional predicted parameters $\chi^{(i)}, n^{(i)}$ dependent on the input $\mathbf{x}^{(i)}$ leading to the updated posterior parameters:

$$\chi^{\text{post},(i)} = \frac{n^{\text{prior}} \chi^{\text{prior}} + n^{(i)} \chi^{(i)}}{n^{\text{prior}} + n^{(i)}}, \quad n^{\text{post},(i)} = n^{\text{prior}} + n^{(i)} \quad (4)$$

Equivalently, NatPN may be interpreted as predicting a set of $n^{(i)}$ pseudo observations $\{y^{(j)}\}_j^{(i)}$ such that their aggregated sufficient statistics satisfy $\sum_j^{(i)} y^{(j)} = n^{(i)} \chi^{(i)}$, and perform the respective Bayesian update. This Bayesian update works for *any* choice of exponential family distributions as long as parameters are mapped to their standard form (see Tab. 1). According to the *principle of maximum entropy* [64], a practical choice for the prior is to enforce high entropy for the prior distribution which is usually considered less informative. It is typically achieved when the prior pseudo-count n^{prior} is small and the prior parameter χ^{prior} accounts for a high aleatoric uncertainty.

Hence, NatPN proposes a generic way to perform the input-dependent Bayesian update $\chi^{(i)}, n^{(i)}$ for *any* exponential family distribution in three steps (see Fig. 2): **(1)** An encoder f_{ϕ} maps the input $\mathbf{x}^{(i)}$ onto a low-dimensional latent vector $\mathbf{z}^{(i)} = f_{\phi}(\mathbf{x}^{(i)}) \in \mathbb{R}^H$ representing useful features for the prediction task (see left Fig.2). Note that the architecture of the encoder can be arbitrarily complex. Then, **(2)** the latent representation $\mathbf{z}^{(i)}$ is used in two different ways to predict the parameter update $\chi^{(i)}$ and the evidence update $n^{(i)}$ (see center Fig.2). On the one hand, a linear decoder g_{ψ} is trained to output the parameter update $\chi^{(i)} = g_{\psi}(\mathbf{z}^{(i)}) \in \mathbb{R}^L$ accounting for the aleatoric uncertainty. On the other hand, a single normalized density is trained to output the evidence update

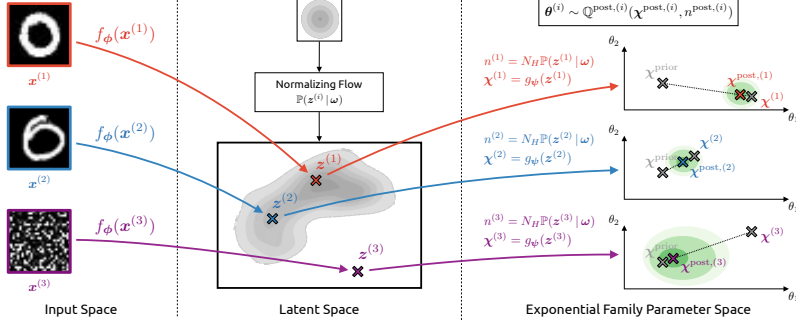


Figure 2: Overview of Natural Posterior Network. Inputs $\mathbf{x}^{(i)}$ are first mapped to a low-dimensional latent representation $\mathbf{z}^{(i)}$ by the encoder f_ϕ . From $\mathbf{z}^{(i)}$, the decoder g_ψ derives the parameter update $\chi^{(i)}$ while a normalizing flow \mathbb{P}_ω yields the evidence update $n^{(i)}$. Posterior parameters are obtained from a weighted combination of prior and update parameters according to $n^{\text{post},(i)}$.

$n^{(i)} = N_H \mathbb{P}(\mathbf{z}^{(i)} | \omega)$ accounting for the epistemic uncertainty. The constant N_H is a certainty budget distributed by the normalized density $\mathbb{P}(\mathbf{z}^{(i)} | \omega)$ over the latent representations $\mathbf{z}^{(i)}$ i.e. $N_H = \int N_H \mathbb{P}(\mathbf{z}^{(i)} | \omega) d\mathbf{z}^{(i)} = \int n^{(i)} d\mathbf{z}^{(i)}$. In practice, we experimented different certainty budget N_H (see app.) and observed that scaling the pseudo-count budget w.r.t. the latent dimension H helped the density to cover larger volumes in higher dimension. Finally, (3) NatPN computes the posterior parameters $\chi^{\text{post},(i)}$ and $n^{\text{post},(i)}$ which can be viewed respectively as the mean and concentration of the posterior distribution (see right Fig.2). Note that the posterior parameter $\chi^{\text{post},(i)}$ is an elegant weighted average of the prior parameter χ^{prior} and the update parameter $\chi^{(i)}$ as shown by Eq. 4.

NatPN extends PostNet [9] which also performs an input-dependent Bayesian update with density estimation. Yet, it has three crucial differences which lead to major practical improvements. First, the new exponential family framework is significantly more flexible and is not restricted to classification. Second, the Dirichlet α parameter computation is different: NatPN computes the χ parameters – which can be viewed as standard softmax output – and the n evidence separately (i.e. $\alpha = n\chi$) while PostNet computes one evidence pseudo-count per class. Third, NatPN architecture is computationally more efficient as it requires a single density contrary to PostNet which requires C densities.

ID and OOD Uncertainty Estimates. NatPN intuitively leads to reasonable uncertainty estimation for the two limit cases of strong ID and OOD inputs (see red and purple samples in Fig. 2). For very likely *in-distribution* data (i.e. $\mathbb{P}(\mathbf{z}^{(i)} | \omega) \rightarrow \infty$), the posterior parameter overrules the prior (i.e. $\chi^{\text{post},(i)} \rightarrow \chi^{(i)}$). Conversely, for very unlikely *out-of-distribution* data (i.e. $\mathbb{P}(\mathbf{z}^{(i)} | \omega) \rightarrow 0$), the prior parameter takes over in the posterior update (i.e. $\chi^{\text{post},(i)} \rightarrow \chi^{\text{prior}}$). Hence, the choice of the prior parameter should reflect the default prediction when the model lacks knowledge. We formally show under mild assumptions on the encoder that NatPN predicts very low additional evidence ($n^{(i)} \approx 0$) for (almost) any input $\mathbf{x}^{(i)}$ far away from the training data (i.e. $\|\mathbf{x}^{(i)}\| \rightarrow +\infty$), thus recovering prior predictions (i.e. $\chi^{\text{post},(i)} \approx \chi^{\text{prior}}$) (see proof in app.).

Theorem 1. Let a NatPN model parametrized with an encoder f_ϕ with piecewise ReLU activations, a decoder g_ψ and the density estimator $\mathbb{P}(\mathbf{z} | \omega)$. Let $f_\phi(\mathbf{x}) = V^{(l)} \mathbf{x} + a^{(l)}$ be the piecewise affine representation of the ReLU network f_ϕ on the finite number of affine regions $Q^{(l)}$ [2]. Suppose that $V^{(l)}$ have independent rows and the density function $\mathbb{P}(\mathbf{z} | \omega)$ has bounded derivatives, then for almost any \mathbf{x} we have $\mathbb{P}(f_\phi(\delta \cdot \mathbf{x}) | \omega) \xrightarrow[\delta \rightarrow \infty]{} 0$. i.e the evidence becomes small far from training data.

This theorem only requires that the density avoids very unlikely pathological behavior with unbounded derivatives [14]. A slightly weaker conclusion holds using the notion of limit in density if the density function does not have bounded derivatives [56]. Finally, the independent rows condition is realistic for trained networks with no constant output [29]. It advantageously leads NatPN to consistent uncertainty estimation contrary to standard ReLU networks which are overconfident [29].

Bayesian NatPN Ensemble. Interestingly, it is natural to extend the Bayesian treatment of a single NatPN to an ensemble of NatPN models. An ensemble of m NatPN models is intuitively equivalent to performing m successive Bayesian updates using each of the NatPN members one after the other. More formally, given an input $\mathbf{x}^{(i)}$ and an ensemble of m jointly trained NatPN

models, the Bayesian update for the posterior distribution becomes $\chi^{\text{post},(i)} = \frac{n^{\text{prior}}\chi^{\text{prior}} + \sum_k^m n_k^{(i)}\chi_k^{(i)}}{n^{\text{prior}} + \sum_k^m n_k^{(i)}}$

and $n^{\text{post},(i)} = n^{\text{prior}} + \sum_k^m n_k^{(i)}$. Note that the standard Bayesian averaging which is used in many ensembling methods [37, 69, 70, 10] is different from this Bayesian combination. While Bayesian averaging assume that only one model is correct, the Bayesian combination of NatPN allows *more* or *none* of the models to be “expert” for some input [49]. For example, an input $\mathbf{x}^{(i)}$ unfamiliar to every model m (i.e. $n_m^{(i)} \approx 0$) would recover the prior default prediction $\chi^{\text{prior}}, n^{\text{prior}}$.

3 Optimization

The choice of the optimization procedure is of primary importance in order to obtain both high-quality target predictions and uncertainty estimates regardless of the task.

Bayesian Loss. We follow [9] and aim at minimizing the following Bayesian loss:

$$\mathcal{L}^{(i)} = - \underbrace{\mathbb{E}_{\boldsymbol{\theta}^{(i)} \sim \mathbb{Q}^{\text{post},(i)}} [\log \mathbb{P}(y^{(i)} | \boldsymbol{\theta}^{(i)})]}_{(1)} - \underbrace{\mathbb{H}[\mathbb{Q}^{\text{post},(i)}]}_{(2)} \quad (5)$$

where $\mathbb{H}[\mathbb{Q}^{\text{post},(i)}]$ denotes the entropy of the predicted posterior distribution $\mathbb{Q}^{\text{post},(i)}$. This loss is guaranteed to be optimal when the predicted posterior distribution is close to the true posterior distribution $\mathbb{Q}^*(\boldsymbol{\theta} | \mathbf{x}^{(i)})$ i.e. $\mathbb{Q}^{\text{post},(i)} \approx \mathbb{Q}^*(\boldsymbol{\theta} | \mathbf{x}^{(i)})$ [5, 66, 76]. The term (1) is the expected likelihood under the predicted posterior distribution. For classification, it can be viewed as an ELBO loss without KL regularization or the Uncertain Cross Entropy (UCE) loss [3] which is known to reduce uncertainty on observed data. The term (2) is an entropy regularizer acting as a prior which favors uninformative distributions $\mathbb{Q}^{\text{post},(i)}$ with high entropy. Observe that this term is not necessarily equal to the prior KL regularization term in the ELBO loss since a proper uniform prior might not exist (e.g. the target y is a real number). When a uniform prior \mathbb{Q}^{unif} exists (e.g. the target y is a class), the loss optimization can be seen as an amortized variational optimization of an ELBO loss [77] i.e. $\mathcal{L}^{(i)} = -\mathbb{E}_{\mathbb{Q}^{\text{post},(i)}} [\log \mathbb{P}(y^{(i)} | \boldsymbol{\theta}^{(i)})] + \text{KL}[\mathbb{Q}^{\text{post},(i)} \| \mathbb{Q}^{\text{unif}}]$ where the predicted distribution $\mathbb{Q}^{\text{post},(i)}$ is the variational distribution — which again approximates the true posterior distribution.

In our case, we restrict the likelihood $\mathbb{P}(y^{(i)} | \boldsymbol{\theta}^{(i)})$ and the posterior $\mathbb{Q}^{\text{post},(i)}$ to be members of the exponential family. We take advantage of the convenient computations for such distributions and derive a more explicit formula for the Bayesian loss of Eq. 5 (see derivation in the appendix):

$$\mathcal{L}^{(i)} \propto \mathbb{E}[\boldsymbol{\theta}]^T \mathbf{u}(y^{(i)}) - \mathbb{E}[A(\boldsymbol{\theta})] - \lambda \mathbb{H}[\mathbb{Q}^{\text{post},(i)}] \quad (6)$$

where λ is an additional regularization weight tuned with a grid search. Note that the term $\mathbb{E}[\boldsymbol{\theta}]^T \mathbf{u}(y^{(i)})$ favors a good alignment of the expected sufficient statistic $\mathbb{E}[\boldsymbol{\theta}] = \chi$ with the observed sufficient statistic $\mathbf{u}(y^{(i)})$. In practice, all terms in Eq. (6) can be computed efficiently and in closed form for most exponential family distributions (see examples in Tab. 1). In particular, further simplifications are possible when the conjugate prior distribution is also in an exponential family which is often the case. Ultimately Eq. (6) applies to *any* exponential family distribution unlike [9].

Optimization Scheme. NatPN is fully differentiable using the closed-form Bayesian loss. Thus, we train the encoder f_ϕ , the parameter decoder g_ψ and the normalizing flow $\mathbb{P}(\mathbf{z}^{(i)} | \boldsymbol{\omega})$ w.r.t. parameters $\phi, \psi, \boldsymbol{\omega}$ jointly. Additionally, we observed that “warm-up” training and “fine-tuning” of the density helped to improve uncertainty estimation for more complex flows and datasets. Thus, we trained the normalizing flow density to maximize the likelihood of the latent representations before and after the joint optimization while keeping all other parameters fixed.

4 Model Limitations

Task-Specific OOD. It has been shown that density estimation is unsuitable for acting on the raw image input [52, 11, 51] or on a non-carefully transformed space [39]. To circumvent this issue, NatPN does not perform OOD detection directly on the input but rather fits a normalizing flow on a learned space. In particular, the latent space is (1) low-dimensional, (2) task-specific and (3) encodes meaningful semantic features. Similarly, [9, 33, 50, 72] already improved OOD detection

of density-based methods by leveraging a task-inductive bias or low-dimensional statistics. In the case of NatPN, the low-dimensional latent space has to contain relevant features to linearly predict the sufficient statistics required for the task. For example, NatPN aims at a linearly separable latent space for classification. The downside is that NatPN is capable of detecting OOD samples only with respect to the considered task and requires labeled examples during training. As an example, NatPN likely fails to detect a change of image color if the task aims at classifying object shapes and the latent space has no notion of color. Hence, we underline that NatPN comes with a task-dependent OOD definition, which is a reasonable choice in practice.

Model-Task Mismatch. Second, we emphasize that the uncertainty estimation quality of NatPN for (close to) ID data depends on the convergence of the model, the encoder architecture (e.g. MLP, Conv., DenseNet) and the target distribution (e.g. Poisson, Normal distributions) choice which should match the task needs. However, we show *empirically* that NatPN provides high quality uncertainty estimates in practice on a wide range of tasks. Further, we show *theoretically* that NatPN leads to uncertain prediction far away from training data for *any* exponential family target distributions. In comparison, [47] showed similar guarantees but for classification only.

5 Experiments

In this section, we compare NatPN to existing methods on extensive experiments including three different tasks: classification, regression and count prediction. For each task type, we evaluate the prediction quality based on target error and uncertainty metrics. These various set-ups aim at proving the versatility of NatPN. In particular, NatPN is the only model that adapts to all tasks and achieving high performances for all metrics without requiring multiple forward passes.

	Accuracy	Brier	9/10 Alea.	9/10 Epist.	OODom Alea.	OODom Epist.
Dropout	98.62 \pm 0.11	3.79 \pm 0.29	30.20 \pm 0.85	32.57 \pm 1.45	27.03 \pm 0.51	95.30 \pm 1.66
Ensemble	98.83 \pm 0.17	3.00 \pm 0.54	30.79 \pm 0.74	32.61 \pm 1.06	27.16 \pm 0.59	99.97 \pm 0.01
NatPE	99.61 \pm 0.03	*0.72 \pm 0.03	87.04 \pm 2.96	68.55 \pm 5.31	99.98 \pm 0.00	*100.00 \pm 0.00
R-PriorNet	98.85 \pm 0.25	2.01 \pm 0.47	40.13 \pm 2.99	30.07 \pm 0.81	*100.00 \pm 0.00	23.59 \pm 0.00
EnID²	93.95 \pm 2.35	28.09 \pm 6.40	26.35 \pm 0.60	24.85 \pm 0.43	84.43 \pm 15.21	23.58 \pm 0.00
PostNet	*99.64 \pm 0.02	0.75 \pm 0.08	80.60 \pm 1.68	*92.57 \pm 1.41	*100.00 \pm 0.00	*100.00 \pm 0.00
NatPN	99.62 \pm 0.03	1.22 \pm 0.19	*87.25 \pm 2.64	79.21 \pm 5.85	99.98 \pm 0.00	*100.00 \pm 0.00

Table 2: Classification results on Sensorless Drive with Categorical target distribution. Best scores among all single-pass models are in bold. Best scores among all models are starred.

	Accuracy	Brier	SVHN Alea.	SVHN Epist.	CelebA Alea.	CelebA Epist.	OODom Alea.	OODom Epist.
Dropout	88.15 \pm 0.20	19.59 \pm 0.41	80.63 \pm 1.59	73.09 \pm 1.51	71.84 \pm 4.28	71.04 \pm 3.92	18.42 \pm 1.11	49.69 \pm 9.10
Ensemble	*89.95 \pm 0.11	17.33 \pm 0.17	85.26 \pm 0.84	82.51 \pm 0.63	76.20 \pm 0.87	74.23 \pm 0.78	25.30 \pm 4.02	89.21 \pm 7.55
NatPE	88.88 \pm 0.13	18.21 \pm 0.26	86.16 \pm 0.24	*83.71 \pm 1.48	*79.34 \pm 0.66	*79.95 \pm 2.80	86.34 \pm 3.95	97.87 \pm 1.22
R-PriorNet	88.94 \pm 0.23	*15.99 \pm 0.32	99.87 \pm 0.02	99.94 \pm 0.01	67.74 \pm 4.86	59.55 \pm 7.90	42.21 \pm 8.77	38.25 \pm 9.82
EnID²	84.03 \pm 0.25	40.84 \pm 0.36	*86.47 \pm 0.66	81.84 \pm 0.92	75.54 \pm 1.79	75.94 \pm 1.82	42.19 \pm 8.77	15.79 \pm 0.27
PostNet	87.95 \pm 0.20	20.19 \pm 0.40	82.35 \pm 0.68	79.24 \pm 1.49	72.96 \pm 2.33	75.84 \pm 1.61	85.89 \pm 4.10	92.30 \pm 2.18
NatPN	88.00 \pm 0.27	20.16 \pm 0.83	82.27 \pm 1.28	79.52 \pm 1.19	76.45 \pm 1.29	75.54 \pm 3.33	*96.90 \pm 1.84	*99.44 \pm 0.32

Table 3: Classification results on CIFAR-10 with Categorical target distribution. Best scores among all single-pass models are in bold. Best scores among all models are starred. Gray numbers indicate that R-PriorNet has seen samples from the SVHN dataset during training.

	RMSE	Calibration	Winter Epist.	Spring Epist.	Autumn Epist.	OODom Epist.
Dropout-\mathcal{N}	70.20 \pm 1.30	6.05 \pm 0.77	15.26 \pm 0.51	13.66 \pm 0.16	15.11 \pm 0.46	99.99 \pm 0.01
Ensemble-\mathcal{N}	*48.02 \pm 2.78	5.88 \pm 1.00	*42.46 \pm 2.29	*21.28 \pm 0.38	21.97 \pm 0.58	*100.00 \pm 0.00
EvReg-\mathcal{N}	49.58 \pm 1.51	3.77 \pm 0.81	17.19 \pm 0.76	15.54 \pm 0.65	14.75 \pm 0.29	34.99 \pm 17.02
NatPN-\mathcal{N}	49.85 \pm 1.28	*2.53 \pm 0.41	39.15 \pm 9.16	20.52 \pm 3.20	*23.08 \pm 2.14	*100.00 \pm 0.00
Dropout-Poi	66.57 \pm 4.61	55.01 \pm 0.19	16.02 \pm 0.48	13.48 \pm 0.38	18.09 \pm 0.82	*100.00 \pm 0.00
Ensemble-Poi	*48.22 \pm 2.06	55.31 \pm 0.21	83.88 \pm 1.22	34.21 \pm 1.81	41.29 \pm 3.23	*100.00 \pm 0.00
NatPN-Poi	52.65 \pm 1.88	*31.57 \pm 1.31	*85.25 \pm 4.53	*34.96 \pm 3.52	*41.72 \pm 7.10	*100.00 \pm 0.00

Table 4: Results on the Bike Sharing Dataset with Normal \mathcal{N} and Poisson Poi target distributions. Best scores among all single-pass models are in bold. Best scores among all models are starred.

5.1 Setup

In our experiments, we change the encoder architecture of **NatPN** to match the dataset needs. We perform a grid search over normalizing flows types (i.e. radial flows [61] and MAF [60, 25]) and latent dimensions. We show further experiments on architecture, latent dimension, normalizing flow choices and certainty budget choice in the appendix. Furthermore, we use approximations of the log-Gamma $\log \Gamma(x)$ and the Digamma $\psi(x)$ functions for large input values to avoid unstable floating

	RMSE	Calibration	Energy Alea.	Energy Epist.	Concrete Alea.	Concrete Epist.	Kin8nm Alea.	Kin8nm Epist.
Dropout	0.09 ± 0.00	3.13 ± 0.43	90.18 ± 6.00	99.94 ± 0.06	$*100.00 \pm 0.00$	$*100.00 \pm 0.00$	in-distribution	
Ensemble	$*0.07 \pm 0.00$	2.69 ± 0.49	$*100.00 \pm 0.00$	$*100.00 \pm 0.00$	$*100.00 \pm 0.00$	$*100.00 \pm 0.00$	in-distribution	
EvReg	0.09 ± 0.00	3.74 ± 0.53	88.06 ± 11.94	88.06 ± 11.94	$*100.00 \pm 0.00$	86.84 ± 13.16	in-distribution	
NatPN	0.08 ± 0.00	$*1.37 \pm 0.54$	$*100.00 \pm 0.00$	$*100.00 \pm 0.00$	$*100.00 \pm 0.00$	$*100.00 \pm 0.00$	in-distribution	
Dropout	$*5.67 \pm 0.07$	$*3.03 \pm 0.40$	9.33 ± 0.36	93.53 ± 2.41	in-distribution		1.09 ± 0.13	64.30 ± 7.14
Ensemble	5.69 ± 0.20	3.81 ± 0.67	54.19 ± 18.93	$*100.00 \pm 0.00$	in-distribution		72.57 ± 19.32	$*100.00 \pm 0.00$
EvReg	6.04 ± 0.18	7.36 ± 1.04	8.93 ± 0.02	51.39 ± 18.56	in-distribution		0.93 ± 0.00	34.44 ± 20.95
NatPN	5.90 ± 0.34	3.89 ± 0.84	$*100.00 \pm 0.00$	$*100.00 \pm 0.00$	in-distribution		$*100.00 \pm 0.00$	$*100.00 \pm 0.00$

Table 5: Regression results on models trained on different UCI datasets with Normal target distribution. The upper half displays models trained on Kin8nm, the lower half shows models trained on Concrete Compressive Strength.

	RMSE	Calibration	LSUN Alea.	LSUN Epist.	KITTI Alea.	KITTI Epist.	OODom Alea.	OODom Epist.
Dropout	46.95	4.03	$*95.29 / 97.74$	$83.89 / 83.22$	98.07	84.90	74.40	$*100.00$
EvReg	28.88	*1.05	58.70 / 56.71	70.19 / 64.02	56.60	62.67	75.43	56.39
NatPN	*27.62	2.84	94.02 / *98.91	*85.19 / *91.11	*99.23	*95.01	*100.00	*100.00

Table 6: Regression results on NYU Depth v2 with Normal target distribution. RMSE is in cm. OOD scores on LSUN are reported on the held-out classes ‘classrooms’ (left) and ‘churches’ (right).

computations (see app.). As prior parameters, we set $\chi^{\text{prior}} = \mathbf{1}_C/C, n^{\text{prior}} = C$ for classification, $\chi^{\text{prior}} = (0, 100)^T, n^{\text{prior}} = 1$ for regression and $\chi^{\text{prior}} = 1, n^{\text{prior}} = 1$ for count prediction.

Baselines. We focus on recent models parametrizing prior distributions over the target distribution. For classification, we compare NatPN to Reverse KL divergence Prior Networks (**R-PriorNet**) [45], Ensemble Distribution Distillation (**EnD**²) [46] and Posterior Networks (**PostNet**) [9]. Note that Prior Networks require OOD training data — we use an auxiliary dataset when available and Gaussian noise otherwise. For regression, we compare to Evidential Regression (**EvReg**) [1]. Beyond baselines parametrizing conjugate prior distributions, we also compare to dropout (**Dropout**) [22] and ensemble (**Ensemble**) [37] models for all tasks. As suggested in [59], we use 5 samples for the two sampling baselines. Note that, unlike the other baselines or NatPN, the sampling baselines require multiple forward passes for uncertainty estimation. In all experiments, all models share the same backbone architecture (MLP, Conv. [74], DenseDepth [17]). We use early stopping and perform a grid search on the hyperparameters of all models including learning rate, dropout rate and regularizing factor when applicable. We report average results over 5 initialization seeds with standard error of the mean (except for the larger dataset NYU Depth v2 dataset). Further model details are given in the appendix.

Datasets. We split all datasets into train, validation and test sets. For classification, we use one tabular dataset (**Sensorless Drive** [15]) and two image datasets (**MNIST** [40] and **CIFAR-10** [34]). For count prediction, we use the **Bike Sharing** dataset [18] to predict the number of rentals within an hour. For regression, we also use the Bike Sharing dataset where the target is viewed as continuous, real-world **UCI datasets** used in [1, 31] and the image **NYU Depth v2** dataset [54] where the goal is to predict the image depth per pixel. All inputs are rescaled with zero mean and unit variance. Similarly, we also scale the output target for regression. Further details are given in the appendix.

Metrics. Beyond the target prediction error, we evaluate model uncertainty estimation using calibration and OOD detection scores. Furthermore, we report the inference speed. Further results including histograms with uncertainty estimates or latent space visualization are presented in appendix. *Target error:* As target prediction scores, we use the accuracy (**Accuracy**) for classification and the Root Mean Squared Error (**RMSE**) for regression and count prediction. *Calibration:* Calibration scores aim at evaluating if the error from the predicted target distribution corresponds to the empirical error achieved by the model (e.g. is a class prediction with a predicted confidence $p_c = 80\%$ correct 80% of the time?). For classification, we use the Brier score (**Brier**) [26]. For regression and count prediction, we use the absolute difference between the percentile p and the percentage p_{pred} of target lying in the confidence interval $I_p = [0, \frac{p}{2}] \cup [1 - \frac{p}{2}, 1]$ under the predicted target distribution. We compute a single calibration score by summing the square difference for $p \in \{0.1, \dots, 0.9\}$ i.e. $\sqrt{\sum_p (p - p_{\text{pred}})^2}$ (**Calibration**) [36]. *OOD detection:* We evaluate how the uncertainty scores enable to detect OOD data using the area under the precision-recall curve (AUC-PR). We show further results using the area under the receiver operating characteristic curve (AUC-ROC) in appendix. We use two different uncertainty measures: the negative entropy of the predicted target distribution accounting for the aleatoric uncertainty (**Alea. OOD**) and the predicted evidence (**Epist. OOD**). Similarly to [59, 9, 45], we use four different types of OOD samples: Unseen datasets (KMNIST [12], Fashion-MNIST [73], SVHN [55], LSUN [75], CelebA [41], KITTI [23]), left-out data (classes 9 and 10 for Sensorless Drive, winter/spring/autumn seasons for Bike Sharing), out-of-domain data which is not normalized in $[0, 1]$ (**OODom**) and dataset shifts (corrupted CIFAR-10 [30]).

5.2 Results

Classification. We show results for the tabular dataset Sensorless Drive with unbounded input domain and the image dataset and CIFAR-10 with bounded input domain are in Tab. 2 and 3. Results for MNIST are in appendix. Overall, for classification NatPN performs on par with best single-pass baselines and NatPE performs the best among multiple-pass models for 19/22 scores. A single NatPN achieves accuracy and calibration performance on par with the most calibrated baselines, namely PostNet and R-PriorNet. Further, NatPE consistently improves accuracy and calibration performances of a single NatPN which underlines the benefit of aggregating multiple models predictions for accuracy and calibration [37]. Without requiring OOD data during training, both NatPN and NatPE achieve excellent OOD detection scores w.r.t. all OOD types. This strongly suggests that NatPN does *not* suffer from the flaws in [52, 11, 51]. In particular, NatPN and NatPE achieve almost perfect OODom scores contrary to all other baselines except PostNet. This observation aligns well with the theoretical guarantee of NatPN far from training data (see Thm. 1) which also applies to each NatPE member. The similar performance of NatPN and PostNet for classification is intuitively explained by their akin design: both models perform density estimation on a low-dimensional latent space. Similarly to [9], we use the average change in confidence as the ratio between the average pseudo-count $\frac{1}{N} \sum_i^N n^{(i)} = \frac{1}{N} \sum_i^N \alpha_0^{(i)}$ at severity 0 vs other severity levels. NatPN maintains a competitive accuracy (Fig. 3, left) while assigning higher epistemic uncertainty as desired (Fig. 3, right). Baselines provide a slower relative confidence decay.

Regression & Count Prediction. We show the results for the Bike Sharing, the tabular UCI datasets and the image NYU Depth v2 datasets in Tab. 4, 5, 6. For the large NYU dataset, we compare against all baselines which require only a single model to be trained. Overall, NatPN outperforms other single-pass models for 24/26 scores for regression, thus significantly improving calibration and OOD detection scores. Further, NatPN shows a strong improvement for calibration and OOD detection for count prediction with Poisson distributions. Interestingly, all the models are less calibrated on the Bike Sharing dataset using a target Poisson distribution rather than a target Normal distribution. This suggests a mismatch of the Poisson distribution for this particular task. The almost perfect OODom scores of NatPN validate again Thm. 1 which also holds for regression.

Inference Speed. We show the average inference time per batch for all models on CIFAR-10 for classification and the NYU Depth v2 dataset for regression in Tab. 4. NatPN shows a significant improvement over Dropout and Ensemble which are both approximately five times slower since they require five forward passes for prediction. Notably, the NatPN speedup does not deteriorate target error and uncertainty scores. NatPN is slightly slower than R-PriorNet, EnD² and EvReg as they do not evaluate an additional normalizing flow. However, NatPN – which uses a single normalizing flow – is faster than PostNet – which scales linearly w.r.t. the number of classes since it evaluates one normalizing flow per class. Lastly, NatPN is the only single-pass model that can be used for both tasks.

6 Conclusion

We introduce a new family of models called Natural Posterior Network which is capable of efficient uncertainty estimation for the wide variety of tasks where the target distribution belongs to the exponential family (incl. classification, regression and count prediction). NatPN relies on the Bayes formula and the general form of the exponential family distribution to perform a closed-form input-dependent posterior update over the target distribution. Further, an ensemble of NatPNs has a principled Bayesian combination interpretation. Theoretically, NatPN guarantees high uncertainty far from training data. Experimentally, NatPN achieves fast, versatile and high-quality uncertainty predictions with strong performance in calibration and OOD detection.

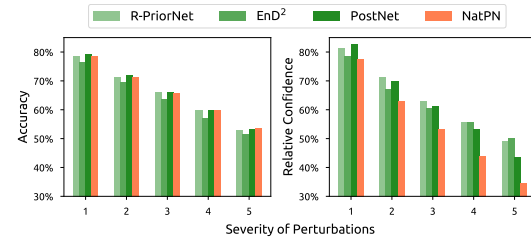


Figure 3: Averaged accuracy and confidence under 15 dataset shifts on CIFAR-10 [30].

	CIFAR-10 (batch size 4,096)	NYU Depth v2 (batch size 4)
Dropout	407.91 ± 5.65	650.96 ± 0.22
Ensemble	361.61 ± 5.41	649.78 ± 0.18
R-PriorNet	61.83 ± 2.57	—
EnD ²	61.83 ± 2.57	—
PostNet	88.56 ± 0.06	—
EvReg	—	129.88 ± 0.75
NatPN	75.64 ± 0.04	137.13 ± 0.18

Figure 4: Batched Inference Time (in ms), NVIDIA GTX 1080 Ti

References

- [1] Alexander Amini, Wilko Schwarting, Ava Soleimany, and Daniela Rus. Deep evidential regression. In *NeurIPS*, 2020.
- [2] Raman Arora, Amitabh Basu, Poorya Mianjy, and Anirbit Mukherjee. Understanding deep neural networks with rectified linear units. In *International Conference on Learning Representations*, 2018.
- [3] Marin Biloš, Bertrand Charpentier, and Stephan Günnemann. Uncertainty on asynchronous time event prediction. In *NeurIPS*, pages 12851–12860, 2019.
- [4] Christopher M Bishop. *Pattern Recognition and Machine Learning*. Springer, 2006.
- [5] P. G. Bissiri, C. C. Holmes, and S. G. Walker. A general framework for updating belief distributions. *Journal of the Royal Statistical Society: Series B (Statistical Methodology)*, 2016.
- [6] Charles Blundell, Julien Cornebise, Koray Kavukcuoglu, and Daan Wierstra. Weight uncertainty in neural networks. In *ICML*, pages 1613–1622, 2015.
- [7] L. D. Brown. *Fundamentals of Statistical Exponential Families: With Applications in Statistical Decision Theory*. Institute of Mathematical Statistics, 1986.
- [8] David M Chan, Roshan Rao, Forrest Huang, and John F Canny. Gpu accelerated t-distributed stochastic neighbor embedding. *JDPC*, pages 1–13, 2019.
- [9] Bertrand Charpentier, Daniel Ziegner, and Stephan Günnemann. Posterior network: Uncertainty estimation without ood samples via density-based pseudo-counts. In *NeurIPS*, 2020.
- [10] Hugh Chipman, Edward George, and Robert Mcculloch. Bayesian ensemble learning. In B. Schölkopf, J. Platt, and T. Hoffman, editors, *NeurIPS*, pages 265–272, 2007.
- [11] Hyunsun Choi, Eric Jang, and Alexander A Alemi. Generative ensembles for robust anomaly detection. In *ICLR*, 2019.
- [12] Tarin Clanuwat, Mikel Bober-Irizar, Asanobu Kitamoto, Alex Lamb, Kazuaki Yamamoto, and David Ha. Deep learning for classical japanese literature. *arXiv preprint arXiv:1812.01718*, 2018.
- [13] Ylvisaker D. Diaconis P. Conjugate priors for exponential families. *The Annals of Statistics*, 1979.
- [14] J. Dix. Existence of the limit at infinity for a function that is integrable on the half line. *Ros-Hulman Undergraduate Mathematics Journal*, 2013.
- [15] Dheeru Dua and Casey Graff. UCI machine learning repository, 2017.
- [16] Michael W. Dusenberry, Ghassen Jerfel, Yeming Wen, Yi-An Ma, Jasper Snoek, Katherine Heller, Balaji Lakshminarayanan, and Dustin Tran. Efficient and scalable bayesian neural nets with rank-1 factors. In *ICML*, 2020.
- [17] David Eigen, Christian Puhrsch, and Rob Fergus. Depth map prediction from a single image using a multi-scale deep network. In *NeurIPS*, pages 2366–2374, 2014.
- [18] Hadi Fanaee-T and João Gama. Event labeling combining ensemble detectors and background knowledge. *Progress in Artificial Intelligence*, 2:113–127, 06 2014.
- [19] Sebastian Farquhar, Lewis Smith, and Yarin Gal. Liberty or depth: Deep bayesian neural nets do not need complex weight posterior approximations. In *Advances in Neural Information Processing Systems*, 2020.
- [20] Andrew Y. K. Foong, David R. Burt, Yingzhen Li, and Richard E. Turner. On the expressiveness of approximate inference in bayesian neural networks. In *NeurIPS*, 2020.
- [21] Yarin Gal. *Uncertainty in Deep Learning*. PhD thesis, University of Cambridge, 2016.
- [22] Yarin Gal and Zoubin Ghahramani. Dropout as a bayesian approximation: Representing model uncertainty in deep learning. In *ICML*, pages 1050–1059, 2016.
- [23] Andreas Geiger, Philip Lenz, Christoph Stiller, and Raquel Urtasun. Vision meets robotics: The kitti dataset. *IJRR*, 2013.
- [24] Andrew Gelman, John B. Carlin, Hal S. Stern, and Donald B. Rubin. *Bayesian Data Analysis*. Chapman and Hall/CRC, 2004.

[25] Mathieu Germain, Karol Gregor, Iain Murray, and Hugo Larochelle. Made: Masked autoencoder for distribution estimation. In *ICML*, pages 881–889, 2015.

[26] Tilmann Gneiting and Adrian E Raftery. Strictly proper scoring rules, prediction, and estimation. *Journal of the American Statistical Association*, 2007.

[27] Alex Graves. Practical variational inference for neural networks. In *NeurIPS*, pages 2348–2356, 2011.

[28] Chuan Guo, Geoff Pleiss, Yu Sun, and Kilian Q. Weinberger. On calibration of modern neural networks. In *ICML*, pages 1321–1330, 2017.

[29] Matthias Hein, Maksym Andriushchenko, and Julian Bitterwolf. Why relu networks yield high-confidence predictions far away from the training data and how to mitigate the problem. 2019.

[30] Dan Hendrycks and Thomas Dietterich. Benchmarking neural network robustness to common corruptions and perturbations. In *ICLR*, 2019.

[31] Jose Miguel Hernandez-Lobato and Ryan Adams. Probabilistic backpropagation for scalable learning of bayesian neural networks. In *ICML*, pages 1861–1869, 2015.

[32] Hyun-Chul Kim and Zoubin Ghahramani. Bayesian classifier combination. In *AISTATS*, pages 619–627, 2012.

[33] Polina Kirichenko, Pavel Izmailov, and Andrew Gordon Wilson. Why normalizing flows fail to detect out-of-distribution data. In *NeurIPS*, 2020.

[34] Alex Krizhevsky, Geoffrey Hinton, et al. Learning multiple layers of features from tiny images. Technical report, University of Toronto, 2009.

[35] Justin Kruger and David Dunning. Unskilled and unaware of it: How difficulties in recognizing one’s own incompetence lead to inflated self-assessments. *JSPS*, 77:1121–1134, 01 2000.

[36] Volodymyr Kuleshov, Nathan Fenner, and Stefano Ermon. Accurate uncertainties for deep learning using calibrated regression. In *ICML*, pages 2796–2804, 2018.

[37] Balaji Lakshminarayanan, Alexander Pritzel, and Charles Blundell. Simple and scalable predictive uncertainty estimation using deep ensembles. In *NeurIPS*, pages 6402–6413, 2017.

[38] Balaji Lakshminarayanan, Dustin Tran, Jeremiah Liu, Shreyas Padhy, Tania Bedrax-Weiss, and Zi Lin. Simple and principled uncertainty estimation with deterministic deep learning via distance awareness. In *NeurIPS*, 2020.

[39] Charline Le Lan and Laurent Dinh. Perfect density models cannot guarantee anomaly detection. *arXiv preprint arXiv:2012.03808*, 2020.

[40] Yann LeCun, Corinna Cortes, and CJ Burges. Mnist handwritten digit database, 2010.

[41] Ziwei Liu, Ping Luo, Xiaogang Wang, and Xiaou Tang. Deep learning face attributes in the wild. In *ICCV*, pages 3730–3738, 2015.

[42] Wesley J Maddox, Pavel Izmailov, Timur Garipov, Dmitry P Vetrov, and Andrew Gordon Wilson. A simple baseline for bayesian uncertainty in deep learning. In *NeurIPS*, pages 13132–13143, 2019.

[43] Andrey Malinin, Sergey Chervontsev, Ivan Prosvirkov, and Mark Gales. Regression prior networks. *arXiv preprint arXiv:2006.11590*, 2020.

[44] Andrey Malinin and Mark Gales. Predictive uncertainty estimation via prior networks. In *NeurIPS*, pages 7047–7058, 2018.

[45] Andrey Malinin and Mark Gales. Reverse kl-divergence training of prior networks: Improved uncertainty and adversarial robustness. In *NeurIPS*, pages 14547–14558, 2019.

[46] Andrey Malinin, Bruno Mlobozeniec, and Mark Gales. Ensemble distribution distillation. *ICLR*, 2020.

[47] Alexander Meinke and Matthias Hein. Towards neural networks that provably know when they don’t know. In *ICLR*, 2020.

[48] Christoph Molnar. Interpretable machine learning, 2020.

[49] K. Monteith, J. L. Carroll, K. Seppi, and T. Martinez. Turning bayesian model averaging into bayesian model combination. In *IJCNN*, 2011.

[50] Warren R. Morningstar, Cusuh Ham, Andrew G. Gallagher, Balaji Lakshminarayanan, Alexander A. Alemi, and Joshua V. Dillon. Density of states estimation for out-of-distribution detection. *arXiv preprint arXiv:2006.09273*, 2020.

[51] Eric Nalisnick, Akihiro Matsukawa, Yee Whye Teh, Dilan Gorur, and Balaji Lakshminarayanan. Do deep generative models know what they don't know? *ICLR*, 2019.

[52] Eric Nalisnick, Akihiro Matsukawa, Yee Whye Teh, and Balaji Lakshminarayanan. Detecting out-of-distribution inputs to deep generative models using typicality. *arXiv preprint arXiv:1906.02994*, 2020.

[53] Jay Nandy, Wynne Hsu, and Mong-Li Lee. Towards maximizing the representation gap between in-domain & out-of-distribution examples. In *NeurIPS*, 2020.

[54] Pushmeet Kohli, Nathan Silberman, Derek Hoiem and Rob Fergus. Indoor segmentation and support inference from rgbd images. In *ECCV*, 2012.

[55] Yuval Netzer, Tao Wang, Adam Coates, Alessandro Bissacco, Bo Wu, and Andrew Y Ng. Reading digits in natural images with unsupervised feature learning. In *NIPS Workshop on Deep Learning and Unsupervised Feature Learning*, 2011.

[56] Constantin P. Niculescu and Florin Popovici. A note on the behavior of integrable functions at infinity. *Journal of Mathematical Analysis and Applications*, 2011.

[57] Frank Nielsen and Richard Nock. Entropies and cross-entropies of exponential families. In *ICIP*, pages 3621–3624, 2010.

[58] Kazuki Osawa, Siddharth Swaroop, Anirudh Jain, Runa Eschenhagen, Richard E. Turner, Rio Yokota, and Mohammad Emtiyaz Khan. Practical deep learning with bayesian principles. *arXiv preprint arXiv:1906.02506*, 2019.

[59] Yaniv Ovadia, Emily Fertig, Jie Ren, Zachary Nado, David Sculley, Sebastian Nowozin, Joshua Dillon, Balaji Lakshminarayanan, and Jasper Snoek. Can you trust your model's uncertainty? evaluating predictive uncertainty under dataset shift. In *NeurIPS*, pages 13991–14002, 2019.

[60] George Papamakarios, Theo Pavlakou, and Iain Murray. Masked autoregressive flow for density estimation. In *NeurIPS*, pages 2338–2347, 2017.

[61] Danilo Jimenez Rezende and Shakir Mohamed. Variational inference with normalizing flows. In *ICML*, volume 37, pages 1530–1538, 2015.

[62] Hippolyt Ritter, Aleksandar Botev, and David Barber. A scalable laplace approximation for neural networks. In *ICLR*, 2018.

[63] Otto Rudolf Rocktäschel. *Methoden zur Berechnung der Gammafunktion für Komplexes Argument*. PhD thesis, Dresden University of Technology, 1922.

[64] R. D. Rosenkrantz. *Prior Probabilities (1968)*, pages 114–130. Springer Netherlands, 1989.

[65] Murat Sensoy, Lance Kaplan, Federico Cerutti, and Maryam Saleki. Uncertainty-aware deep classifiers using generative models. *AAAI Conference on Artificial Intelligence*, pages 5620–5627, 2020.

[66] John Shawe-Taylor and Robert C. Williamson. A pac analysis of a bayesian estimator. In *COLT*, pages 2–9, 1997.

[67] Weishi Shi, Xujiang Zhao, Feng Chen, and Qi Yu. Multifaceted uncertainty estimation for label-efficient deep learning. In *NeurIPS*, 2020.

[68] Edwin Simpson, Stephen Roberts, Ioannis Psorakis, and Arfon Smith. Dynamic bayesian combination of multiple imperfect classifiers, 2012.

[69] Yeming Wen, Dustin Tran, and Jimmy Ba. Batchensemble: an alternative approach to efficient ensemble and lifelong learning. In *ICLR*, 2020.

[70] Florian Wenzel, Jasper Snoek, Dustin Tran, and Rodolphe Jenatton. Hyperparameter ensembles for robustness and uncertainty quantification. *NeurIPS*, 2020.

[71] E.T. Whittaker and G.N. Watson. *A Course of Modern Analysis*. Cambridge University Press, 4th edition, 1927.

- [72] Jim Winkens, Rudy Bunel, Abhijit Guha Roy, Robert Stanforth, Vivek Natarajan, Joseph R. Ledsam, Patricia MacWilliams, Pushmeet Kohli, Alan Karthikesalingam, Simon Kohl, Taylan Cemgil, S. M. Ali Eslami, and Olaf Ronneberger. Contrastive training for improved out-of-distribution detection. *arXiv preprint arXiv:2007.05566*, 2020.
- [73] Han Xiao, Kashif Rasul, and Roland Vollgraf. Fashion-mnist: a novel image dataset for benchmarking machine learning algorithms. *arXiv preprint arXiv:1708.07747*, 2017.
- [74] Rikiya Yamashita, Mizuho Nishio, Richard Do, and Kaori Togashi. Convolutional neural networks: an overview and application in radiology. *Insights into Imaging*, 9, 2018.
- [75] Fisher Yu, Yinda Zhang, Shuran Song, Ari Seff, and Jianxiong Xiao. Lsun: Construction of a large-scale image dataset using deep learning with humans in the loop. *arXiv preprint arXiv:1506.03365*, 2015.
- [76] Arnold Zellner. Optimal information processing and bayes's theorem. *The American Statistician*, page 278, 11 1988.
- [77] Cheng Zhang, Judith Bütepage, Hedvig Kjellström, and Stephan Mandt. Advances in variational inference. *IEEE TPAMI*, pages 2008–2026, 2018.
- [78] Xujiang Zhao, Feng Chen, Shu Hu, and Jin-Hee Cho. Uncertainty aware semi-supervised learning on graph data. In *NeurIPS*, 2020.

A Proofs

We prove theorem 1 based on Lemmas 2 and 3. Lemma 2 states that the latent space can be divided in a finite number of linear regions [2]. Lemma 3 states that a probability density with bounded derivatives has to converge to 0 at infinity [14]. We additionally provide 4 which provide a similar convergence guarantee without the bounded derivative constraint [56]. Finally, Lemma 5 particularly shows that the guarantee of theorem 1 can be obtained with Gaussian Mixtures which are commonly used for density estimation or radial flows which are used in the experiments.

Lemma 2. [2] Let $\{Q_l\}_l^R$ be the set of linear regions associated to the piecewise ReLU network $f_\phi(\mathbf{x})$. For any $\mathbf{x} \in \mathbb{R}^D$, there exists $\delta^* \in \mathbb{R}^+$ and $l^* \in 1, \dots, R$ such that $\delta\mathbf{x} \in Q_{l^*}$ for all $\delta > \delta^*$.

Lemma 3. [14] Let $p \in L^1(0, \infty)$ with bounded first derivative p' , then $p(\delta) \xrightarrow{\delta \rightarrow \infty} 0$. This convergence is stronger than in Lem. 4 as the limit is not in density but with standard limit notation.

Lemma 4. [56] Let $p \in L^1(0, \infty)$, then $p(\delta) \xrightarrow{\delta \rightarrow \infty} 0$ in density. This means that the sets where $p(t)$ is far from its 0 limit (i.e. $\{\alpha \geq: |p(t)| \geq \epsilon\}$ with $\epsilon > 0$) has zero density.

Lemma 5. Let $\mathbb{P}(\mathbf{z} | \omega)$ be parametrized with a Gaussian Mixture Model (GMM) or a radial flow, then $\mathbb{P}(\mathbf{z} | \omega) \xrightarrow{\|\mathbf{z}\| \rightarrow \infty} 0$.

Proof. We prove now lem. 5 for GMM and radial flow. The proof is straightforward for the GMM parametrization since every Gaussian component of the mixture has 0 limit when $\|\mathbf{z}\| \rightarrow \infty$.

Let denote now $p_1(\mathbf{z}) = \mathbb{P}(\mathbf{z} | \omega)$ be parametrized with a radial flow transformation $g(\mathbf{z})$ and a base unit Gaussian distribution p_0 i.e.:

$$p_1(\mathbf{z}) = p_0(g(\mathbf{z})) \times \left| \det \frac{\partial g(\mathbf{z})}{\partial \mathbf{z}} \right|$$

Further, we can express the transformation $g(\mathbf{z})$ and its determinant $\det \frac{\partial g(\mathbf{z})}{\partial \mathbf{z}}$ as follows:

$$\begin{aligned} g(\mathbf{z}) &= \mathbf{z} + \beta h(\alpha, r)(\mathbf{z} - \mathbf{z}_0) \\ \det \frac{\partial g(\mathbf{z})}{\partial \mathbf{z}} &= \frac{1 + \beta h(\alpha, r) + \beta h'(\alpha, r)r}{(1 + \beta h(\alpha, r))^{H-1}} \end{aligned}$$

where $h(\alpha, r) = \frac{1}{\alpha+r}$ and $r = \|\mathbf{z} - \mathbf{z}_0\|$. On one hand, we have $\|g(\mathbf{z})\| \rightarrow +\infty$ when $\|\mathbf{z}\| \rightarrow \infty$ since $\|\beta h(\alpha, r)(\mathbf{z} - \mathbf{z}_0)\| < \beta$. Thus, the base Gaussian density $p_0(g(\mathbf{z})) \rightarrow 0$ when $\|\mathbf{z}\| \rightarrow \infty$. On the other hand, we have $\left| \det \frac{\partial g(\mathbf{z})}{\partial \mathbf{z}} \right| \rightarrow 1$ since $\beta h(\alpha, r) \rightarrow 0$ and $\beta h'(\alpha, r)r \rightarrow 0$ when $\|\mathbf{z}\| \rightarrow \infty$. Therefore, the transformed density $p_0(g(\mathbf{z})) \times \left| \det \frac{\partial g(\mathbf{z})}{\partial \mathbf{z}} \right| \rightarrow 0$ when $\|\mathbf{z}\| \rightarrow \infty$ which ended the proof. Note that this proof can be extended to stacked radial flows by induction. \square

Theorem. Let a NatPN model parametrized with an encoder f_ϕ with piecewise ReLU activations, a decoder g_ψ and the density estimator $\mathbb{P}(\mathbf{z} | \omega)$. Let $f_\phi(\mathbf{x}) = V^{(l)}\mathbf{x} + a^{(l)}$ be the piecewise affine representation of the ReLU network f_ϕ on the finite number of affine regions $Q^{(l)}$ [2]. Suppose that $V^{(l)}$ have independent rows and the density function $\mathbb{P}(\mathbf{z} | \omega)$ has bounded derivatives, then for almost any \mathbf{x} we have $\mathbb{P}(f_\phi(\delta \cdot \mathbf{x}) | \omega) \xrightarrow{\delta \rightarrow \infty} 0$. i.e the evidence becomes small far from training data.

Proof. We prove now thm. 1. Let $\mathbf{x} \in \mathbb{R}^D$ be a non-zero input and f_ϕ be a ReLU network. Lem. 2 implies that there exists $\delta^* \in \mathbb{R}^+$ and $l \in \{1, \dots, R\}$ such that $\delta \cdot \mathbf{x} \in Q^{(l)}$ for all $\delta > \delta^*$. Thus, $\mathbf{z}_\delta = f_\phi(\delta \cdot \mathbf{x}) = \delta \cdot (V^{(l)}\mathbf{x} + a^{(l)})$ for all $\delta > \delta^*$. Note that for $\delta \in [\delta^*, +\infty]$, \mathbf{z}_δ follows an affine half line $S_{\mathbf{x}} = \{\mathbf{z} | \mathbf{z} = \delta \cdot (V^{(l)}\mathbf{x} + a^{(l)}, \delta > \delta^*)\}$ in the latent space. Further, note that $V^{(l)}\mathbf{x} \neq 0$ and $\|\mathbf{z}_\delta\| \xrightarrow{\delta \rightarrow \infty} +\infty$ since $\mathbf{x} \neq 0$ and $V^{(l)}$ has independent rows.

We now define the function $p(\delta) = \mathbb{P}(\mathbf{z}_\delta | \omega)$ which is the density function $\mathbb{P}(\mathbf{z} | \omega)$ restricted on the affine half line $S_{\mathbf{x}}$. Since $\mathbb{P}(\mathbf{z} | \omega)$ is a normalized probability density, then the function $\delta \mapsto p(\delta - \delta^*)$

is integrable on $[0, +\infty]$. Indeed we have:

$$\begin{aligned} \int_0^{+\infty} p(\delta - \delta^*) d\delta &= \int_{\delta^*}^{+\infty} p(\delta) d\delta \\ &= \int_{\delta^*}^{+\infty} \mathbb{P}(\delta \cdot (V^{(l)} \mathbf{x}) + a^{(l)} | \boldsymbol{\omega}) d\delta \\ &= \int_{S_{\mathbf{x}}} \mathbb{P}(\mathbf{z} | \boldsymbol{\omega}) d\mathbf{z} < +\infty \end{aligned}$$

Further since the function $\mathbb{P}(\mathbf{z} | \boldsymbol{\omega})$ has bounded derivatives, we can apply Lem. 3 to the function $\delta \mapsto p(\delta - \delta^*)$ to get the expected result i.e.

$$\mathbb{P}(f_{\phi}(\delta \cdot \mathbf{x}) | \boldsymbol{\omega}) = p(\delta) = p((\delta + \delta^*) - \delta^*) \xrightarrow{\delta \rightarrow \infty} 0$$

which ends the proof.

Alternatively a slightly weaker conclusion also holds if the density function does not have bounded derivatives using lem. 4 (instead of lem. 3) with the notion of limit in density. The stronger conclusion is valid if we parametrize $\mathbb{P}(\mathbf{z} | \boldsymbol{\omega})$ with a Gaussian Mixture Model or a radial flow density according to lem. 5 since $\|\mathbf{z}_{\delta}\| \xrightarrow{\delta \rightarrow \infty} +\infty$. \square

B Formulae for Exponential Family Distributions

B.1 General Case

Target Distribution. An exponential family distribution on a target variable $y \in \mathbb{R}$ with natural parameters $\boldsymbol{\theta} \in \mathbb{R}^L$ can be denoted as

$$\mathbb{P}(y | \boldsymbol{\theta}) = h(y) \exp(\boldsymbol{\theta}^T \mathbf{u}(y) - A(\boldsymbol{\theta})) \quad (7)$$

where $h : \mathbb{R} \rightarrow \mathbb{R}$ is the carrier measure, $A : \mathbb{R}^L \rightarrow \mathbb{R}$ the log-normalizer and $\mathbf{u} : \mathbb{R} \rightarrow \mathbb{R}^L$ the sufficient statistics.

Conjugate Prior Distribution. An exponential family distribution \mathbb{P} always admits a conjugate prior:

$$\mathbb{Q}(\boldsymbol{\theta} | \boldsymbol{\chi}, n) = \eta(\boldsymbol{\chi}, n) \exp(n \boldsymbol{\theta}^T \boldsymbol{\chi} - n A(\boldsymbol{\theta})) \quad (8)$$

where $\eta : \mathbb{R}^L \times \mathbb{R} \rightarrow \mathbb{R}$ is a normalization factor and A the log-normalizer of the distribution \mathbb{P} as in Eq. 7).

Posterior Predictive Distribution. The posterior predictive distribution is given as $\int \mathbb{P}(y^{(i)} | \boldsymbol{\theta}) \mathbb{Q}(\boldsymbol{\theta} | \boldsymbol{\chi}^{post, (i)}, n^{post, (i)}) d\boldsymbol{\theta}$ where the parameter $\boldsymbol{\theta}$ is marginalized out [21]. This distribution can always be computed in closed form for exponential family distributions:

$$\mathbb{P}(y | \boldsymbol{\chi}, n) = h(y) \frac{\eta(\boldsymbol{\chi}, n)}{\eta\left(\frac{n\boldsymbol{\chi} + \mathbf{u}(y)}{n+1}, n+1\right)} \quad (9)$$

where h is the carrier measure defined in Eq. 7 and η is the normalization factor defined in Eq. 8. In particular, the posterior predictive distributions for Categorical, Normal and Poisson target distributions are Categorical, Student and Negative Binomial distributions, respectively.

Likelihood. The log-likelihood of an exponential family distribution can be written as follows:

$$\log \mathbb{P}(y^{(i)} | \boldsymbol{\theta}) = \log h(y^{(i)}) + \boldsymbol{\theta}^T \mathbf{u}(y^{(i)}) - A(\boldsymbol{\theta}) \quad (10)$$

Expected Log-Likelihood. Given the log-likelihood of an exponential family distribution, its expectation under the conjugate prior distribution $\mathbb{Q}(\boldsymbol{\theta} | \boldsymbol{\chi}, n)$ can be written as

$$\mathbb{E}_{\boldsymbol{\theta} \sim \mathbb{Q}(\boldsymbol{\chi}, n)} [\log \mathbb{P}(y^{(i)} | \boldsymbol{\theta})] = \log h(y^{(i)}) + \mathbb{E}_{\boldsymbol{\theta} \sim \mathbb{Q}(\boldsymbol{\chi}, n)} [\boldsymbol{\theta}]^T \mathbf{u}(y^{(i)}) - \mathbb{E}_{\boldsymbol{\theta} \sim \mathbb{Q}(\boldsymbol{\chi}, n)} [A(\boldsymbol{\theta})] \quad (11)$$

where $\mathbb{E}_{\mathbb{Q}(\boldsymbol{\theta} | \boldsymbol{\chi}, n)} [\boldsymbol{\theta}] = \boldsymbol{\chi}$ [7, 13].

Entropy. The entropy of a random variable $y \sim \mathbb{P}(\boldsymbol{\theta})$ for an exponential family distribution \mathbb{P} can be written as follows [57]:

$$\mathbb{H}[\mathbb{P}(\boldsymbol{\theta})] = A(\boldsymbol{\theta}) - \boldsymbol{\theta}^T \nabla_{\boldsymbol{\theta}} A(\boldsymbol{\theta}) - \mathbb{E}_{y \sim \mathbb{P}(\boldsymbol{\theta})} [\log h(y)] \quad (12)$$

B.2 Categorical & Dirichlet Distributions

The Dirichlet distribution $\mathbf{p} \sim \text{Dir}(\boldsymbol{\alpha})$ is the conjugate prior of the categorical distributions $\mathbf{y} \sim \text{Cat}(\mathbf{p})$.

Target Distribution. The density and the entropy of the categorical distribution are:

$$\text{Cat}(\mathbf{y} \mid \mathbf{p}) = \sum_{i=1}^K \mathbb{I}[y_i = 1] p_i \quad (13)$$

$$\mathbb{H}[\text{Cat}(\mathbf{p})] = \sum_{c=1}^C \log p_c \quad (14)$$

Conjugate Prior Distribution. The density and the entropy of the Dirichlet distribution are:

$$\text{Dir}(\mathbf{p} \mid \boldsymbol{\alpha}) = \frac{\Gamma\left(\sum_{c=1}^C \alpha_c\right)}{\prod_{c=1}^C \Gamma(\alpha_c)} \prod_{c=1}^C p_c^{\alpha_c-1} \quad (15)$$

$$\mathbb{H}[\text{Dir}(\boldsymbol{\alpha})] = \log B(\boldsymbol{\alpha}^{(i)}) + (\alpha_0^{(i)} - C)\psi(\alpha_0^{(i)}) - \sum_c (\alpha_c^{(i)} - 1)\psi(\alpha_c^{(i)}) \quad (16)$$

where $\psi(\alpha)$ and $B(\alpha)$ denote Digamma and Beta functions, respectively, and $\alpha_0 = \sum_c \alpha_c$.

Expected Log-Likelihood. The expected likelihood of the categorical distribution $\text{Cat}(\mathbf{p})$ under the Dirichlet distribution $\text{Dir}(\boldsymbol{\alpha})$ is

$$\mathbb{E}_{\mathbf{p} \sim \text{Dir}(\boldsymbol{\alpha})}[\log \text{Cat}(\mathbf{y} \mid \mathbf{p})] = \psi(\alpha_y) - \psi(\alpha_0) \quad (17)$$

where $\psi(\alpha)$ denotes Digamma function.

B.3 Normal & Normal-Inverse-Gamma Distributions

The Normal-Inverse-Gamma (NIG) distribution $\mu, \sigma \sim \mathcal{N}\Gamma^{-1}(\mu_0, \lambda, \alpha, \beta)$ is the conjugate prior of the normal distribution $\mathbf{y} \sim \mathcal{N}(\mu, \sigma)$. Note that as both parameters λ and α can be viewed as pseudo-counts. However, the natural prior parametrization enforces a single pseudo-count n corresponding to $\lambda = 2\alpha$.

Target Distribution. The density and the entropy of the Normal distribution are:

$$\mathcal{N}(\mathbf{y} \mid \mu, \sigma) = \frac{1}{\sigma\sqrt{2\pi}} \exp\left(-\frac{(x - \mu)^2}{2\sigma^2}\right) \quad (18)$$

$$\mathbb{H}[\mathcal{N}(\mu, \sigma)] = \frac{1}{2} \log(2\pi\sigma^2) \quad (19)$$

Conjugate Prior Distribution. The density and the entropy of the NIG distribution are:

$$\mathcal{N}\Gamma^{-1}(\mu, \sigma \mid \mu_0, \lambda, \alpha, \beta) = \frac{\beta^\alpha \sqrt{\lambda}}{\Gamma(\alpha) \sqrt{2\pi\sigma^2}} \left(\frac{1}{\sigma^2}\right)^{\alpha+1} \exp\left(-\frac{2\beta + \lambda(\mu - \mu_0)^2}{2\sigma^2}\right) \quad (20)$$

$$\mathbb{H}[\mathcal{N}\Gamma^{-1}(\mu_0, \lambda, \alpha, \beta)] = \frac{1}{2} + \log\left((2\pi)^{\frac{1}{2}}\beta^{\frac{3}{2}}\Gamma(\alpha)\right) - \frac{1}{2} \log \lambda + \alpha - \left(\alpha + \frac{3}{2}\right) \psi(\alpha) \quad (21)$$

where $\Gamma(\alpha)$ denotes the Gamma function.

Expected Log-Likelihood. The expected likelihood of the Normal distribution $\mathcal{N}(\mu, \sigma)$ under the NIG distribution $\mathcal{N}\Gamma^{-1}(\mu_0, \lambda, \alpha, \beta)$ is:

$$\mathbb{E}_{(\mu, \sigma) \sim \mathcal{N}\Gamma^{-1}(\mu_0, \lambda, \alpha, \beta)}[\log \mathcal{N}(y | \mu, \sigma)] \quad (22)$$

$$= \mathbb{E} \left[-\frac{(y - \mu)^2}{2\sigma^2} - \log(\sigma\sqrt{2\pi}) \right] \quad (23)$$

$$= \frac{1}{2} \left(-\mathbb{E} \left[\frac{(y - \mu_0)^2}{2\sigma^2} \right] - \mathbb{E} [\log \sigma^2] - \log 2\pi \right) \quad (24)$$

$$= \frac{1}{2} \left(-y^2 \mathbb{E} \left[\frac{1}{\sigma^2} \right] + 2y \mathbb{E} \left[\frac{\mu}{\sigma^2} \right] - \mathbb{E} \left[\frac{\mu^2}{\sigma^2} \right] + \mathbb{E} \left[\log \frac{1}{\sigma^2} \right] - \log 2\pi \right) \quad (25)$$

$$= \frac{1}{2} \left(-\frac{\alpha}{\beta} (y - \mu_0)^2 - \frac{1}{\lambda} + \psi(\alpha) - \log \beta - \log 2\pi \right) \quad (26)$$

where $\psi(\alpha)$ denotes the Digamma function. We used here the moments of the NIG distribution $\mathbb{E} \left[\frac{\mu}{\sigma^2} \right] = \frac{\alpha\mu_0}{\beta}$, $\mathbb{E} \left[\frac{1}{\sigma^2} \right] = \frac{\alpha}{\beta}$, $\mathbb{E} \left[\frac{\mu^2}{\sigma^2} \right] = \frac{\alpha\mu_0^2}{\beta} + \frac{1}{\lambda}$, and the moment of the inverse Gamma distribution $\mathbb{E} [\log \frac{1}{\sigma^2}] = \psi(\alpha) - \log \beta$.

B.4 Poisson & Gamma Distributions

The Gamma distribution $\lambda \sim \Gamma(\alpha, \beta)$ is the conjugate prior of the Poisson distributions $y \sim \text{Poi}(\lambda)$.

Target Distribution. The density and the entropy of the Poisson distribution are:

$$\text{Poi}(y | \lambda) = \frac{\lambda^y \exp(-\lambda)}{y!} \quad (27)$$

$$\mathbb{H}[\text{Poi}(\lambda)] = \lambda(1 - \log(\lambda)) + \exp(-\lambda) \sum_{k=0}^{\infty} \frac{\lambda^k \log(k!)}{k!} \quad (28)$$

Conjugate Prior Distribution. The density and the entropy of the Gamma distribution are:

$$\Gamma(\lambda | \alpha, \beta) = \frac{\beta^\alpha}{\Gamma(\alpha)} \lambda^{\alpha-1} \exp(-\beta\lambda) \quad (29)$$

$$\mathbb{H}[\Gamma(\alpha, \beta)] = \alpha + \log \Gamma(\alpha) - \log \beta + (1 - \alpha)\psi(\alpha) \quad (30)$$

where $\Gamma(\alpha)$ denotes the Gamma function.

Expected Log-Likelihood. The expected likelihood of the Poisson distribution $\text{Poi}(\lambda)$ under the Gamma distribution $\Gamma(\alpha, \beta)$ is

$$\mathbb{E}_{\lambda \sim \Gamma(\alpha, \beta)}[\log \text{Poi}(y | \lambda)] = \mathbb{E}[\log \lambda]y - \mathbb{E}[\lambda] - \sum_{k=1}^y \log k \quad (31)$$

$$= (\psi(\alpha) - \log \beta)y - \frac{\alpha}{\beta} - \sum_{k=1}^y \log k \quad (32)$$

where $\psi(\alpha)$ denotes Digamma function. We used here the moments the Gamma distributions $\mathbb{E}[\log \lambda] = \psi(\alpha) - \log \beta$ and $\mathbb{E}[\lambda] = \frac{\alpha}{\beta}$. Note that $\sum_{k=1}^y \log k$ is constant w.r.t. parameters α, β .

C Approximation of Entropies

The computation of a distribution's entropy often requires subtracting huge numbers from each other. While these numbers tend to be very close together, this introduces numerical challenges. For large parameter values, we therefore approximate the entropy by substituting numerically unstable terms and simplifying the resulting formula. For this procedure, we make use of the following equivalences (taken from [63] and [71], respectively):

$$\log \Gamma(x) \approx \frac{1}{2} \log 2\pi - x + \left(x - \frac{1}{2} \right) \log x \quad (33)$$

$$\psi(x) = \log x - \frac{1}{2x} + \mathcal{O}\left(\frac{1}{x^2}\right) \quad (34)$$

We note that Eq. 34 especially implies $\psi(x) \approx \log x$ and $x\psi(x) \approx x \log x - \frac{1}{2}$ for large x .

C.1 Dirichlet Distribution

We consider a Dirichlet distribution $\text{Dir}(\boldsymbol{\alpha})$ of order K with $\alpha_0 = \sum_{i=1}^K \alpha_i$. For $\alpha_0 \geq 10^4$, we use the following approximation:

$$\mathbb{H}[\text{Dir}(\boldsymbol{\alpha})] \approx \frac{K-1}{2}(1 + \log 2\pi) + \frac{1}{2} \sum_{i=1}^K \log \alpha_i - \left(K - \frac{1}{2}\right) \log \sum_{i=1}^K \alpha_i \quad (35)$$

C.2 Normal-Inverse-Gamma Distribution

We consider a Normal-Inverse-Gamma distribution $\mathcal{N}\Gamma^{-1}(\mu, \lambda, \alpha, \beta)$. For $\alpha \geq 10^4$, we use the following approximation:

$$\mathbb{H}[\mathcal{N}\Gamma^{-1}(\mu, \lambda, \alpha, \beta)] \approx 1 + \log 2\pi - 2 \log \alpha + \frac{3}{2} \log \beta - \frac{1}{2} \log \lambda \quad (36)$$

C.3 Gamma Distribution

We consider a Gamma distribution $\Gamma(\alpha, \beta)$. For $\alpha \geq 10^4$, we use the following approximation:

$$\mathbb{H}[\Gamma(\alpha, \beta)] \approx \frac{1}{2} + \frac{1}{2} \log 2\pi + \frac{1}{2} \log \alpha - \log \beta \quad (37)$$

D Formulae for Uncertainty Estimates

Aleatoric Uncertainty. The entropy of the target distribution $\mathbb{P}(\boldsymbol{\theta})$ was used to estimate the aleatoric uncertainty i.e. $\mathbb{H}[\mathbb{P}(\boldsymbol{\theta})]$.

Epistemic Uncertainty. The evidence parameter $n^{\text{post},(i)}$ was used to estimate the epistemic uncertainty. Due to its interpretation as a pseudo-count of observed labels, the posterior evidence parameter is indeed a natural indicator for the epistemic uncertainty.

Predictive Uncertainty. The entropy of the posterior distribution $\mathbb{Q}(\boldsymbol{\theta}|\boldsymbol{\chi}^{\text{post},(i)}, n^{\text{post},(i)})$ was used to estimate the predictive uncertainty.

E Dataset Details

We use a train/validation/test split in all experiments. For datasets with a dedicated test split, we split the rest of the data into training and validation sets of size 80%/20%. For all other datasets, we used 70%/15%/15% for the train/validation/test sets. All inputs are rescaled with zero mean and unit variance. Similarly, we also scale the output target for regression.

Sensorless Drive [15] This is a tabular dataset where the goal is to classify extracted motor current measurements into 11 different classes. We remove the last two classes (9 and 10) from training and use them as the OOD dataset for OOD detection experiments. Each input is composed of 48 attributes describing motor behavior. The dataset contains 58,509 samples in total.

MNIST [40] This is an image dataset where the goal is to classify pictures of hand-drawn digits into 10 classes (from digit 0 to digit 9). Each input is composed of a $1 \times 28 \times 28$ tensor. The dataset contains 70,000 samples. For OOD detection experiments, we use KMNIST [12] and Fashion-MNIST [73] containing images of Japanese characters and images of clothes, respectively.

CIFAR-10 [34] This is an image dataset where the goal is to classify a picture of objects into 10 classes (airplane, automobile, bird, cat, deer, dog, frog, horse, ship, truck). Each input is a $3 \times 32 \times 32$ tensor. The dataset contains 60,000 samples. For OOD detection experiments, we use street view

house numbers (SVHN) [55] containing images of numbers and CelebA [41] containing images of celebrity faces. Furthermore, we generate the corrupted CIFAR-10 dataset [30] with 15 corruption types per image, each with 5 different severities.

Bike Sharing [18] This is a tabular dataset where the goal is to predict the total number of rentals within an hour. Each input is composed of 15 attributes. We removed features related to the year period (i.e. record index, date, season, months) which would make OOD detection trivial, leading to 11 attributes. The dataset contains 17,389 samples in total. For OOD detection, we removed the attribute season from the input data and only trained on the summer season. The samples related to winter, spring and autumn were used as OOD datasets.

Concrete [15] This is a tabular dataset where the goal is to predict the compressive strength of high-performance concrete. Each input is composed of 8 attributes. The dataset contains 1,030 samples in total. For OOD detection, we use the Energy and Kin8nm datasets which have the same input size.

Kin8nm [15] This is a tabular dataset where the goal is to predict the forward kinematics of an 8-link robot arm. Each input is composed of 8 attributes. The dataset contains 8,192 samples in total. For OOD detection, we the Concrete and Energy datasets which have the same input size.

NYU Depth v2 [54] This is an image dataset where the goal is to predict the depth of room images at each pixel position. All inputs are of shape 3x640x480 tensors while we rescale outputs to be 320x240 tensors. The dataset contains 50,000 samples in total available on the DenseDepth GitHub². For OOD detection, we use the KITTI [23] dataset containing images of driving cars and two out of the 20 categories from the LSUN [75] dataset.

F Model Details

We train all models using 5 seeds except for the large NYU dataset where we use a single randomly selected seed. All models are optimized with the Adam optimizer without further learning rate scheduling. We perform early stopping by checking loss improvement every epoch and a patience p selected per dataset (Sensorless Drive: $p = 15$, MNIST: $p = 15$, CIFAR10: $p = 20$, Bike Sharing: $p = 50$, Concrete: $p = 50$, Kin8nm: $p = 30$, NYU Depth v2: $p = 2$). We train all models on a single GPU (NVIDIA GTX 1080 Ti or NVIDIA GTX 2080 Ti, 11 GB memory). All models are trained after a grid search for the learning rate in $[1e^{-2}, 5e^{-4}]$. The backbone architecture is shared across models and selected per dataset to match the task needs (Sensorless Drive: 3 lin. layers with 64 hidden dim, MNIST: 6 conv. layers with 32/32/32/64/64/64 filters + 3 lin. layers with hidden dim 1024/128/64, CIFAR10: 8 conv. layers with 32/32/32/64/64/128/128/128 filters + 3 lin. layers with hidden dim 1024/128/64, Bike Sharing: 3 lin. layers with 16/16/16 hidden dim, Concrete: 2 lin. layers with 16/16 hidden dim, Kin8nm: 2 lin. layers with 16/16 hidden dim, NYU Depth v2: DenseDepth + 4 upsampling layers with convolutions and skip connections). For the NYU Depth v2 dataset, we use a pretrained DenseNet for initialization of the backbone architecture which was fine-tuned during training. The remaining layers are trained from scratch. All architectures use LeakyReLU activations.

Baselines. For the dropout models, we use the best drop out rate p_{drop} per dataset after a grid search in $\{0.1, 0.25, 0.4\}$ and sample 5 times for uncertainty estimation. Similarly, we use $m = 5$ for the ensemble baseline and the distribution distillation. Note that [59] found that a relative small ensemble size (e.g. $m = 5$) may indeed be sufficient in practice. We also train Prior Networks where we set $\beta_{\text{in}} = 1e^2$ as suggested in the original papers [44, 45]. Prior Networks use Fashion-MNIST and SVHN as training OOD datasets for MNIST and CIFAR-10, respectively. As there is no available OOD dataset for the Sensorless Drive dataset, we use Gaussian noise as training OOD data.

Natural Posterior Network. We perform a grid search for the entropy regularizer in the range $[1e^{-5}, 0]$, for the latent dimension in $\{4, 8, 16, 32\}$, and for normalizing flow type between radial flows [61] with 8, 16 layers and Masked Autoregressive flows [60, 25] with 4, 8, 16 layers. The certainty budget is set such that $\log N_H = \frac{1}{2}(H \log(2\pi) + \log(H + 1))$ which helps to cover larger volumes in higher dimensions. Further results on latent dimensions, density types, number of normalizing flow layers and certainty budget are presented in Sec. H.5. We use “warm-up” training for the normalizing flows for all datasets except for the simple Concrete and Kin8nm datasets, and the NYU Depth v2 dataset which starts from a pretrained encoder. We use “fine-tuning” for the normalizing

²<https://github.com/ialhashim/DenseDepth>

flows for all datasets except for the simple Concrete and Kin8nm datasets. As prior parameters, we set $\chi^{\text{prior}} = \mathbf{1}_C/C$, $n^{\text{prior}} = C$ for classification, $\chi^{\text{prior}} = (0, 100)^T$, $n^{\text{prior}} = 1$ for regression and $\chi^{\text{prior}} = 1$, $n^{\text{prior}} = 1$ for count prediction. Note that the mean of these prior distributions correspond to an equiprobable Categorical distribution $\text{Cat}(\mathbf{1}_C/C)$, a Normal distribution with large variance $\mathcal{N}(0, 10)$ and a Poisson distribution with a unitary mean $\text{Poi}(1)$. Those prior target distributions represent the safe default prediction when no evidence is predicted.

G Experiment Details

Target Error Metric. For classification, we use the standard accuracy $\frac{1}{N} \sum_i \mathbb{I}[\mathbf{y}^{*,(i)} = \mathbf{y}^{(i)}]$ where $\mathbf{y}^{*,(i)}$ is the one-hot true label and $\mathbf{y}^{(i)}$ is the one-hot predicted label. For regression, we use the standard Root Mean Square Error $\sqrt{\frac{1}{N} \sum_i^N (\mathbf{y}^{*,(i)} - \mathbf{y}^{(i)})^2}$.

Calibration Metric. For classification, we use the Brier score which is computed as $\frac{1}{C} \sum_i^N \|\mathbf{p}^{(i)} - \mathbf{y}^{(i)}\|_2$ where $\mathbf{p}^{(i)}$ is the predicted softmax probability and $\mathbf{y}^{(i)}$ is the one-hot encoded ground-truth label. For regression and count prediction, we use the absolute difference between the percentile p and the percentage of target lying in the confidence interval $I_p = [0, \frac{p}{2}] \cup [1 - \frac{p}{2}, 1]$ under the predicted target distribution. Formally, we compute $p_{\text{pred}} = \frac{1}{N} \sum_i \mathbb{I}[F_{\theta^{(i)}}(\mathbf{y}^{*,(i)}) \in I_p]$ where $F_{\theta^{(i)}}(\mathbf{y}^{*,(i)}) = \mathbb{P}(y \leq \mathbf{y}^{*,(i)} | \theta^{(i)})$ is the cumulative function of the predicted target distribution evaluated at the true target. For example, the percentile $p = 0.1$ would be compared to $p_{\text{pred}} = \frac{1}{N} \sum_i \mathbb{I}[F_{\theta^{(i)}}(\mathbf{y}^{*,(i)})] \in [0, 0.05] \cup [0.95, 1]$ which should be close to 0.10 for calibrated predictions. We compute a single calibration score by summing the square difference for $p \in \{0.1, \dots, 0.9\}$ i.e. $\sqrt{\sum_p (p - p_{\text{pred}})^2}$ [36].

OOD Metric. The OOD detection task can be evaluated as a binary classification. Hence, we assign class 1 to ID data and class 0 to OOD data task and use the aleatoric and epistemic uncertainty estimates as scores for OOD data. It enables to compute final scores using the area under the precision-recall curve (AUC-PR) and the area under the receiver operating characteristic curve (AUC-ROC). Both metrics have been scaled by 100. We obtain numbers in $[0, 100]$ for all scores instead of $[0, 1]$. Results for AUC-ROC are reported in Sec. H.6.

Inference Time Metric. We measure inference time of models in ms and used NVIDIA GTX 1080 Ti GPUs. We evaluate the inference for one classification dataset (CIFAR-10) and one regression dataset (NYU Depth v2). For evaluation, we use a randomly initialized model and simply push random data through the model with batch size of 4,096 CIFAR10 and batch size of 4 for NYU Depth v2. The final numbers are averaged over 100 batches excluding the first batch due to GPU initialization. Compared models shared the same backbone architecture.

H Additional Experiments

H.1 MNIST results

	Accuracy	Brier	K. Alea.	K. Epist.	F. Alea.	F. Epist.	OODom Alea.	OODom Epist.
Dropout	99.45 \pm 0.01	1.07 \pm 0.05	98.27 \pm 0.05	97.82 \pm 0.08	99.40 \pm 0.03	98.01 \pm 0.14	43.86 \pm 1.62	74.09 \pm 0.92
Ensemble	*99.46 \pm 0.02	1.02 \pm 0.02	98.39 \pm 0.07	98.43 \pm 0.05	99.33 \pm 0.06	98.73 \pm 0.08	40.98 \pm 1.80	66.54 \pm 0.58
NatPE	99.44 \pm 0.02	1.02 \pm 0.03	98.77 \pm 0.33	*99.50 \pm 0.03	*99.42 \pm 0.07	*99.68 \pm 0.01	*100.00 \pm 0.00	*100.00 \pm 0.00
R-PriorNet	99.35 \pm 0.04	*0.97 \pm 0.03	*99.33 \pm 0.18	99.28 \pm 0.25	100.00 \pm 0.00	100.00 \pm 0.00	97.48 \pm 0.66	31.03 \pm 0.13
End²	99.24 \pm 0.05	6.19 \pm 0.13	98.36 \pm 0.15	98.76 \pm 0.13	99.25 \pm 0.16	99.35 \pm 0.14	48.09 \pm 1.38	31.60 \pm 0.39
PostNet	99.44 \pm 0.04	1.79 \pm 0.42	98.86 \pm 0.11	98.44 \pm 0.16	98.92 \pm 0.18	98.65 \pm 0.25	*100.00 \pm 0.00	*100.00 \pm 0.00
NatPN	99.35 \pm 0.03	1.38 \pm 0.06	98.66 \pm 0.20	98.52 \pm 0.67	99.27 \pm 0.12	99.08 \pm 0.42	99.96 \pm 0.01	*100.00 \pm 0.00

Table 7: Results on MNIST (classification with Categorical target distribution). Best scores among all single-pass models are in bold. Best scores among all models are starred. Gray numbers indicate that R-PriorNet has seen samples from the FMNIST dataset during training.

H.2 Latent Space Visualizations

We propose additional visualizations of the latent space for MNIST with t-SNE [8] with different perplexities (see Fig. 5). For all perplexities, we clearly observe ten green clusters corresponding to

the ten classes for MNIST. The KMNIST (OOD) samples in red can easily be separated from the MNIST (ID) samples in green. As desired, NatPN assigns higher log-probabilities used in evidence computation to ID samples from MNIST.

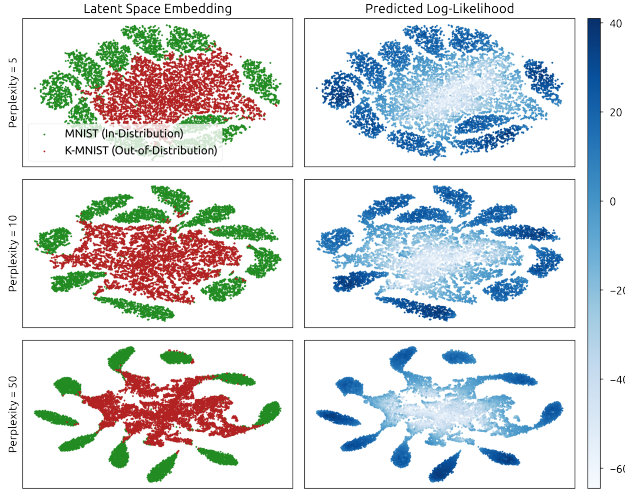


Figure 5: t-SNE visualization of the latent space of NatPN on MNIST (ID) vs KMNIST (OOD). On the left, The ID data (MNIST in green) can easily be distinguished from the OOD data (KMNIST in red). On the right, NatPN correctly assigns higher likelihood to ID data.

H.3 Histogram of Uncertainty Estimates

We visualize the histogram distribution of the entropy of the posterior distribution accounting for predictive uncertainty for ID (MNIST/NYU) and OOD (KNMIST and Fashion-MNIST/LSUN classroom and LSUN church + KITTI) (see Fig. 6). We clearly observe lower predictive entropy for ID data than for OOD data for both MNIST and NYU datasets. On one hand, the entropy clearly differentiates between ID data (MNIST) and any other OOD datasets (KMNIST, Fashion MNIST, OODom) for classification. We intuitively explain this clear distinction since the samples from the OOD datasets are irrelevant for the digit classification task. On the other hand, the entropy is still a good indicator of ID (NYU) and OOD datasets (LSUN classroom and LSUN church + KITTI) for regression although the distinction between ID and OOD datasets is less strong compared to MNIST. We intuitively explain this behavior since the task of depth estimation is still relevant to LSUN classroom and LSUN church + KITTI. Interestingly, as the NYU dataset contains indoor pictures, the entropy of OOD indoor pictures (i.e. LSUN classroom) have lower entropy than OOD outdoor pictures (LSUN church + KITTI).

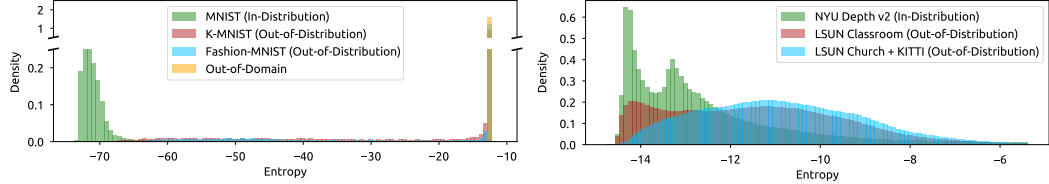


Figure 6: Histogram of the entropy of the posterior distribution accounting for the predictive uncertainty of NatPN on MNIST (ID) vs KMNIST, Fashion-MNIST, Out-Of-Domain (OOD) and NYU (ID) vs LSUN classroom and LSUN church + KITTI (OOD). In both cases, low entropy is a good indicator of in-distribution data.

H.4 Uncertainty Visualization on NYU Depth v2 Dataset

We visualize the prediction and the predictive uncertainty per pixel for the NYU Depth v2 dataset (see Fig. 7). We observe accurate target predictions compared to the ground truth depth of the images.

Further NatPN assigns higher uncertainty for pixels close to object edges, which is reasonable since the depth abruptly change at these locations.

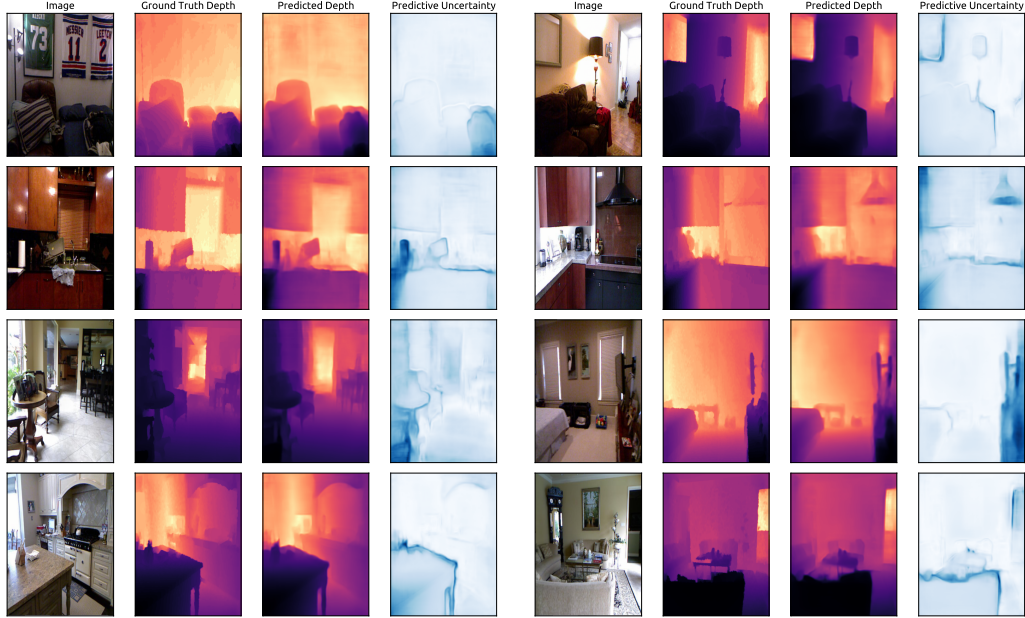


Figure 7: Visualization of the predicted depth and predictive uncertainty estimates of NatPN per pixel on the NYU Depth v2 dataset. NatPN predicts accurate depth uncertainty and reasonably assigns higher uncertainty to object edges.

H.5 Hyper-Parameter Study

As an ablation study, we also report the results of the grid search on the latent dimension, normalizing flow types and number of normalizing flow layers for MNIST, CIFAR-10 and Bike Sharing datasets in Tab. 8, 10, 12. While most models converge to fairly good uncertainty estimates, we notice that 16 layers of simple radial flows on latent spaces of 16 dimensions were achieving very good results in practice. Changing the flow type or the number of normalizing flow layers does not lead to strong variations of the results except for Bike sharing with Poisson target distributions. In this case, more complex MAF normalizing flows improve NatPN performance. The latent dimension appears to be a more important choice for the model convergence. As an example, a higher latent dimension of 16 or 32 leads to significantly better performances than a latent dimension of 4 on MNIST, CIFAR10 and Bike Sharing datasets. We hypothesize that too low latent dimensions are less able to encode the necessary information for the prediction task, leading to worse target errors.

Further, we compare three different variants of the certainty budget N_H used in the evidence computation $n^{(i)} = N_H \mathbb{P}(z^{(i)} | \omega)$: a constant unit budget (i.e. $N_H = 1$) corresponding to a fixed budget regardless of the number of training data and the latent dimension, a budget equals to the number of training data (i.e. $N_H = N$) similarly to [9], or a budget which scales exponentially (or faster) with the number of latent dimensions (i.e. $\log N_H = \frac{1}{2}(H \log(2\pi) + \log(H+1))$). We observe that scaling the budget w.r.t. the latent space dimension (H -budget) is more stable in practice than constant budget (1-budget) and budget related to the number of training data (N -budget) (see. Tab. 9,11,13,15). The H -budget achieves significantly better target error scores for CIFAR-10 and Bike Sharing with Poisson targets and performance on par with the other certainty budget scheme otherwise. The intuition is that due to the curse of dimensionality, the expected value of a probability density function $\mathbb{E}_z[\mathbb{P}(z)]$ tends to decrease exponentially fast. For example, we have $\mathbb{E}_z[\mathbb{P}(z)] = \frac{1}{(\sqrt{4\pi})^H}$ when $z \sim \mathcal{N}(\mathbf{0}, \mathbf{1})$ in a H -dimensional space. Increasing the certainty budget N_H exponentially (or faster) w.r.t. to the dimension H avoids numerical issues by allocating close to 0 evidence to latent representations. In our experiments, we use $\log N_H = \frac{1}{2}(H \log(2\pi) + \log(H+1))$.

H.6 OOD Detection with AUC-ROC Scores

In addition to the AUC-APR scores, we report the OOD detection results for MNIST, CIFAR10 and Bike Sharing datasets in Tab. 16, 17, 18, 19 with AUC-ROC scores. Similarly as with AUC-APR scores, NatPN and NatPE achieve very competitive performances compare to the baselines. It particular, they outperform all baselines to detect challenging OODom data.

	Accuracy	Brier	K. Alea.	K. Epist.	F. Alea.	F. Epist.	OODom Alea.	OODom Epist.
NatPN (4 - 8/0)	83.28 \pm 2.08	41.21 \pm 2.73	91.09 \pm 0.62	85.02 \pm 0.97	91.76 \pm 1.36	84.27 \pm 0.65	*100.00 \pm 0.00	*100.00 \pm 0.00
NatPN (4 - 16/0)	83.46 \pm 2.37	36.60 \pm 2.70	95.74 \pm 0.35	96.20 \pm 0.45	97.41 \pm 0.53	97.04 \pm 0.36	*100.00 \pm 0.00	*100.00 \pm 0.00
NatPN (4 - 0/4)	97.40 \pm 0.78	17.82 \pm 6.11	98.69 \pm 0.21	96.71 \pm 0.81	99.43 \pm 0.12	98.41 \pm 0.78	99.80 \pm 0.04	*100.00 \pm 0.00
NatPN (4 - 0/8)	96.09 \pm 1.52	25.57 \pm 8.28	98.14 \pm 0.36	97.04 \pm 1.01	99.19 \pm 0.16	98.72 \pm 0.59	99.86 \pm 0.03	*100.00 \pm 0.00
NatPN (4 - 0/16)	98.30 \pm 0.19	8.10 \pm 0.81	*99.04 \pm 0.19	98.32 \pm 0.49	*99.47 \pm 0.06	*99.35 \pm 0.16	99.78 \pm 0.04	*100.00 \pm 0.00
NatPN (16 - 8/0)	99.34 \pm 0.02	1.57 \pm 0.16	96.82 \pm 0.52	80.57 \pm 1.25	96.98 \pm 0.66	78.75 \pm 2.06	*100.00 \pm 0.00	*100.00 \pm 0.00
NatPN (16 - 16/0)	*99.35 \pm 0.03	*1.38 \pm 0.06	98.66 \pm 0.20	*98.52 \pm 0.67	99.27 \pm 0.12	99.08 \pm 0.42	99.96 \pm 0.01	*100.00 \pm 0.00
NatPN (16 - 0/4)	99.23 \pm 0.04	1.89 \pm 0.10	98.49 \pm 0.08	95.34 \pm 0.84	99.14 \pm 0.11	96.24 \pm 1.19	99.95 \pm 0.01	*100.00 \pm 0.00
NatPN (16 - 0/8)	99.24 \pm 0.03	1.95 \pm 0.13	98.64 \pm 0.11	96.57 \pm 0.26	99.17 \pm 0.13	97.84 \pm 0.51	99.94 \pm 0.01	*100.00 \pm 0.00
NatPN (16 - 0/16)	99.20 \pm 0.04	1.99 \pm 0.10	98.63 \pm 0.07	97.47 \pm 0.17	99.21 \pm 0.10	98.51 \pm 0.36	99.93 \pm 0.02	*100.00 \pm 0.00
NatPN (32 - 8/0)	99.33 \pm 0.02	1.56 \pm 0.06	96.12 \pm 0.42	73.55 \pm 1.40	97.64 \pm 0.72	73.24 \pm 1.64	*100.00 \pm 0.00	*100.00 \pm 0.00
NatPN (32 - 16/0)	*99.35 \pm 0.03	3.73 \pm 2.08	96.03 \pm 1.61	88.85 \pm 3.60	96.83 \pm 1.46	89.15 \pm 3.66	*100.00 \pm 0.00	*100.00 \pm 0.00
NatPN (32 - 0/4)	99.16 \pm 0.04	1.64 \pm 0.09	98.48 \pm 0.10	96.92 \pm 0.20	99.01 \pm 0.09	98.11 \pm 0.14	99.96 \pm 0.01	*100.00 \pm 0.00
NatPN (32 - 0/8)	99.17 \pm 0.03	1.66 \pm 0.03	98.47 \pm 0.04	97.26 \pm 0.26	99.15 \pm 0.07	98.25 \pm 0.31	99.97 \pm 0.01	*100.00 \pm 0.00
NatPN (32 - 0/16)	99.16 \pm 0.02	1.66 \pm 0.08	98.35 \pm 0.09	97.60 \pm 0.07	98.88 \pm 0.15	97.98 \pm 0.30	99.99 \pm 0.00	*100.00 \pm 0.00

Table 8: MNIST Comparison (<latent dim> – <radial layers>/<MAF layers>). Bold and starred number indicate best score among all models.

	Accuracy	Brier	K. Alea.	K. Epist.	F. Alea.	F. Epist.	OODom Alea.	OODom Epist.
NatPN (1-budget)	*99.51 \pm 0.01	*1.22 \pm 0.10	99.23 \pm 0.13	99.41 \pm 0.02	99.24 \pm 0.08	99.38 \pm 0.04	*100.00 \pm 0.00	*100.00 \pm 0.00
NatPN (N-budget)	99.40 \pm 0.03	1.24 \pm 0.05	*99.42 \pm 0.03	*99.44 \pm 0.02	*99.44 \pm 0.06	*99.53 \pm 0.05	99.99 \pm 0.00	*100.00 \pm 0.00
NatPN (H-budget)	99.35 \pm 0.03	1.38 \pm 0.06	98.66 \pm 0.20	98.52 \pm 0.67	99.27 \pm 0.12	99.08 \pm 0.42	99.96 \pm 0.01	*100.00 \pm 0.00

Table 9: MNIST Comparison N_H Scaling. Bold and starred number indicate best score among all models.

	Accuracy	Brier	SVHN Alea.	SVHN Epist.	CelebA Alea.	CelebA Epist.	OODom Alea.	OODom Epist.
NatPN (4 - 8/0)	85.11 \pm 0.77	35.95 \pm 1.57	75.20 \pm 3.03	53.51 \pm 3.95	72.14 \pm 7.01	54.96 \pm 5.53	68.68 \pm 4.06	70.52 \pm 2.40
NatPN (4 - 16/0)	84.11 \pm 1.12	33.67 \pm 2.37	77.65 \pm 1.72	63.36 \pm 3.68	*77.02 \pm 1.44	58.50 \pm 4.32	90.86 \pm 4.89	90.20 \pm 4.93
NatPN (4 - 0/4)	77.02 \pm 2.04	58.05 \pm 9.43	61.10 \pm 7.36	27.78 \pm 3.73	63.37 \pm 5.78	27.79 \pm 2.49	99.44 \pm 0.36	99.69 \pm 0.28
NatPN (4 - 0/8)	72.98 \pm 2.74	49.01 \pm 4.32	69.83 \pm 3.76	30.71 \pm 5.16	69.45 \pm 3.25	35.15 \pm 4.97	99.81 \pm 0.09	99.97 \pm 0.02
NatPN (16 - 8/0)	88.17 \pm 0.15	19.89 \pm 0.39	84.16 \pm 0.55	59.14 \pm 1.21	75.37 \pm 2.31	66.35 \pm 2.14	88.23 \pm 2.06	76.22 \pm 7.46
NatPN (16 - 16/0)	88.00 \pm 0.27	20.16 \pm 0.83	82.27 \pm 1.28	*79.52 \pm 1.19	76.45 \pm 1.29	*75.54 \pm 3.33	96.90 \pm 1.84	99.44 \pm 0.32
NatPN (16 - 0/4)	88.01 \pm 0.30	19.71 \pm 0.39	*84.96 \pm 0.82	70.04 \pm 3.65	74.65 \pm 1.35	65.01 \pm 3.16	99.08 \pm 0.87	99.97 \pm 0.03
NatPN (16 - 0/8)	*88.41 \pm 0.14	*19.01 \pm 0.22	81.87 \pm 0.73	74.09 \pm 1.74	75.91 \pm 2.15	69.21 \pm 1.57	99.21 \pm 0.69	99.98 \pm 0.02
NatPN (32 - 8/0)	87.89 \pm 0.09	19.92 \pm 0.19	82.44 \pm 1.61	48.41 \pm 3.47	75.72 \pm 1.81	57.49 \pm 1.80	97.29 \pm 1.03	90.62 \pm 5.01
NatPN (32 - 16/0)	87.74 \pm 0.15	20.59 \pm 0.34	82.98 \pm 0.60	58.07 \pm 4.59	75.06 \pm 1.17	66.54 \pm 3.37	97.29 \pm 1.13	99.02 \pm 0.37
NatPN (32 - 0/4)	87.90 \pm 0.21	20.03 \pm 0.36	84.20 \pm 0.52	64.71 \pm 2.31	73.69 \pm 1.86	63.75 \pm 3.14	*99.84 \pm 0.12	*100.00 \pm 0.00
NatPN (32 - 0/8)	88.16 \pm 0.15	19.46 \pm 0.27	82.04 \pm 1.83	65.84 \pm 2.21	74.28 \pm 1.92	55.58 \pm 2.85	99.67 \pm 0.16	*100.00 \pm 0.00

Table 10: CIFAR-10 Comparison (<latent dim> – <radial layers>/<MAF layers>). Bold and starred number indicate best score among all models.

	Accuracy	Brier	SVHN Alea.	SVHN Epist.	CelebA Alea.	CelebA Epist.	OODom Alea.	OODom Epist.
NatPN (1-budget)	84.04 \pm 1.33	27.88 \pm 2.42	82.33 \pm 1.20	71.79 \pm 2.09	74.17 \pm 2.95	63.32 \pm 1.38	95.65 \pm 3.76	97.97 \pm 1.52
NatPN (N -budget)	87.13 \pm 0.44	21.37 \pm 0.73	*82.70 \pm 1.35	75.73 \pm 2.87	*79.23 \pm 1.06	*78.98 \pm 1.80	96.02 \pm 1.66	98.71 \pm 0.51
NatPN (H -budget)	*88.00 \pm 0.27	*20.16 \pm 0.83	82.27 \pm 1.28	*79.52 \pm 1.19	76.45 \pm 1.29	75.54 \pm 3.33	*96.90 \pm 1.84	*99.44 \pm 0.32

Table 11: CIFAR-10 Comparison N_H Scaling. Bold and starred number indicate best score among all models.

	RMSE	Calibration	Winter Epist.	Spring Epist.	Autumn Epist.	OODom Epist.
NatPN (4 – 8/0)	52.81 \pm 2.43	21.75 \pm 1.84	20.12 \pm 0.43	15.62 \pm 0.37	17.95 \pm 0.26	*100.00 \pm 0.00
NatPN (4 – 16/0)	51.87 \pm 3.52	22.96 \pm 0.98	20.94 \pm 0.79	14.96 \pm 0.33	18.98 \pm 1.31	*100.00 \pm 0.00
NatPN (4 – 0/4)	64.26 \pm 10.56	23.95 \pm 1.02	26.45 \pm 0.65	16.46 \pm 0.58	18.98 \pm 1.37	*100.00 \pm 0.00
NatPN (4 – 0/8)	63.09 \pm 8.16	24.13 \pm 0.71	38.24 \pm 6.09	18.47 \pm 1.09	21.78 \pm 1.94	*100.00 \pm 0.00
NatPN (4 – 0/16)	73.99 \pm 9.85	24.68 \pm 1.67	35.99 \pm 3.88	20.40 \pm 1.51	21.49 \pm 1.07	*100.00 \pm 0.00
NatPN (16 – 8/0)	51.11 \pm 1.24	*2.32 \pm 0.41	25.89 \pm 5.12	16.57 \pm 1.23	19.57 \pm 2.73	*100.00 \pm 0.00
NatPN (16 – 16/0)	50.30 \pm 2.49	4.44 \pm 1.09	25.92 \pm 2.76	17.03 \pm 0.91	18.63 \pm 1.30	*100.00 \pm 0.00
NatPN (16 – 0/4)	*48.75 \pm 2.14	3.18 \pm 0.63	29.97 \pm 1.75	17.91 \pm 0.82	22.76 \pm 1.85	*100.00 \pm 0.00
NatPN (16 – 0/8)	54.15 \pm 3.08	3.07 \pm 0.52	*40.58 \pm 7.10	20.51 \pm 1.60	*24.69 \pm 4.73	*100.00 \pm 0.00
NatPN (16 – 0/16)	49.85 \pm 1.28	2.53 \pm 0.41	39.15 \pm 9.16	*20.52 \pm 3.20	23.08 \pm 2.14	*100.00 \pm 0.00
NatPN (32 – 8/0)	52.80 \pm 2.51	4.09 \pm 0.94	26.85 \pm 2.82	16.76 \pm 0.92	17.30 \pm 1.53	*100.00 \pm 0.00
NatPN (32 – 16/0)	55.67 \pm 4.29	3.15 \pm 0.72	27.53 \pm 3.28	17.40 \pm 0.80	18.64 \pm 0.81	*100.00 \pm 0.00
NatPN (32 – 0/4)	50.50 \pm 1.29	3.72 \pm 0.72	26.15 \pm 6.27	16.65 \pm 2.07	18.43 \pm 1.10	*100.00 \pm 0.00
NatPN (32 – 0/8)	52.20 \pm 3.16	2.80 \pm 0.72	25.95 \pm 5.84	16.17 \pm 1.34	20.79 \pm 2.80	*100.00 \pm 0.00
NatPN (32 – 0/16)	50.61 \pm 1.72	2.38 \pm 0.76	20.92 \pm 3.44	14.17 \pm 0.88	19.68 \pm 2.58	*100.00 \pm 0.00

Table 12: Bike Sharing (Normal \mathcal{N}) Comparison (<latent dim> – <radial layers>/<MAF layers>). Bold and starred number indicate best score among all models.

	RMSE	Calibration	Winter Epist.	Spring Epist.	Autumn Epist.	OODom Epist.
NatPN (1-budget)	*49.22 \pm 1.58	3.38 \pm 0.72	23.54 \pm 3.14	15.46 \pm 0.89	19.76 \pm 1.48	*100.00 \pm 0.00
NatPN (N -budget)	54.50 \pm 4.78	*1.95 \pm 0.49	33.17 \pm 7.40	18.79 \pm 2.29	20.87 \pm 1.74	*100.00 \pm 0.00
NatPN (H -budget)	49.85 \pm 1.28	2.53 \pm 0.41	*39.15 \pm 9.16	*20.52 \pm 3.20	*23.08 \pm 2.14	*100.00 \pm 0.00

Table 13: Bike Sharing (Normal \mathcal{N}) Comparison N_H Scaling. Bold and starred number indicate best score among all models.

	RMSE	Winter Epist.	Spring Epist.	Autumn Epist.	Winter OODom Epist.
NatPN (4 – 8/0)	15878.27 \pm 9480.29	21.35 \pm 3.08	14.00 \pm 0.58	17.51 \pm 1.22	*100.00 \pm 0.00
NatPN (4 – 16/0)	18534.26 \pm 9295.93	31.88 \pm 4.38	17.90 \pm 0.90	22.61 \pm 2.16	*100.00 \pm 0.00
NatPN (4 – 0/4)	179635.99 \pm 93952.22	42.26 \pm 8.69	19.42 \pm 2.11	23.29 \pm 1.68	*100.00 \pm 0.00
NatPN (4 – 0/8)	45382.86 \pm 22573.84	54.55 \pm 9.79	22.81 \pm 2.72	34.32 \pm 5.10	*100.00 \pm 0.00
NatPN (4 – 0/16)	52011.84 \pm 15966.07	60.11 \pm 7.21	25.57 \pm 1.92	25.55 \pm 1.53	*100.00 \pm 0.00
NatPN (16 – 8/0)	2322.25 \pm 1505.61	33.35 \pm 5.24	18.40 \pm 1.96	24.66 \pm 3.21	*100.00 \pm 0.00
NatPN (16 – 16/0)	2875.78 \pm 1336.66	48.02 \pm 6.85	21.68 \pm 1.73	32.12 \pm 4.34	*100.00 \pm 0.00
NatPN (16 – 0/4)	52.65 \pm 1.88	85.25 \pm 4.53	34.96 \pm 3.52	41.72 \pm 7.10	*100.00 \pm 0.00
NatPN (16 – 0/8)	62.97 \pm 13.91	82.10 \pm 3.20	*35.39 \pm 3.61	*43.33 \pm 5.66	*100.00 \pm 0.00
NatPN (16 – 0/16)	52.25 \pm 1.47	68.14 \pm 9.41	31.83 \pm 2.72	29.99 \pm 6.08	*100.00 \pm 0.00
NatPN (32 – 8/0)	52.07 \pm 1.10	47.53 \pm 7.40	21.82 \pm 1.57	29.98 \pm 5.71	*100.00 \pm 0.00
NatPN (32 – 16/0)	49.37 \pm 1.63	59.66 \pm 7.89	26.61 \pm 5.37	34.29 \pm 4.62	*100.00 \pm 0.00
NatPN (32 – 0/4)	*49.08 \pm 1.80	68.83 \pm 9.31	26.00 \pm 3.84	42.78 \pm 5.77	*100.00 \pm 0.00
NatPN (32 – 0/8)	50.89 \pm 1.24	*85.39 \pm 3.99	31.88 \pm 2.19	41.68 \pm 3.15	*100.00 \pm 0.00
NatPN (32 – 0/16)	50.33 \pm 3.16	68.93 \pm 7.99	32.00 \pm 4.80	32.74 \pm 4.13	*100.00 \pm 0.00

Table 14: Bike Sharing (Poisson Poi) Comparison (<latent dim> – <radial layers>/<MAF layers>). Bold and starred number indicate best score among all models.

	RMSE	Winter Epist.	Spring Epist.	Autumn Epist.	Winter OODom Epist.
NatPN (1-budget)	87.86 \pm 29.81	72.27 \pm 4.95	29.31 \pm 3.71	40.86 \pm 3.62	*100.00 \pm 0.00
NatPN (N -budget)	172.25 \pm 73.44	*88.19 \pm 2.34	*39.23 \pm 2.97	41.81 \pm 5.16	*100.00 \pm 0.00
NatPN (H -budget)	*52.65 \pm 1.88	85.25 \pm 4.53	34.96 \pm 3.52	41.72 \pm 7.10	*100.00 \pm 0.00

Table 15: Bike Sharing (Poisson Poi) Comparison N_H Scaling. Bold and starred number indicate best score among all models.

	K. Alea.	K. Epist.	F. Alea.	F. Epist.	OODom Alea.	OODom Epist.
Dropout	98.12 \pm 0.05	97.16 \pm 0.11	99.26 \pm 0.03	96.87 \pm 0.25	15.19 \pm 1.70	88.16 \pm 0.59
Ensemble	98.17 \pm 0.07	98.03 \pm 0.05	99.15 \pm 0.07	98.04 \pm 0.11	11.83 \pm 1.81	81.53 \pm 0.38
NatPE	98.86 \pm 0.15	99.39 \pm 0.04	*99.32 \pm 0.08	*99.62 \pm 0.02	*100.00 \pm 0.00	*100.00 \pm 0.00
R-PriorNet	*99.44 \pm 0.09	*99.59 \pm 0.08	100.00 \pm 0.00	100.00 \pm 0.00	99.44 \pm 0.16	1.82 \pm 0.67
EnD²	98.21 \pm 0.16	98.65 \pm 0.15	99.06 \pm 0.20	99.21 \pm 0.17	56.31 \pm 2.78	4.60 \pm 1.89
PostNet	98.79 \pm 0.10	98.50 \pm 0.12	98.75 \pm 0.20	98.54 \pm 0.21	*100.00 \pm 0.00	*100.00 \pm 0.00
NatPN	98.67 \pm 0.12	98.03 \pm 1.01	99.20 \pm 0.12	98.89 \pm 0.52	99.93 \pm 0.03	*100.00 \pm 0.00

Table 16: MNIST - OOD detection with AUC-ROC scores. Bold numbers indicate best score among single-pass models. Starred numbers indicate best scores among all models. Gray numbers indicate that R-PriorNet has seen samples from the Fashion-MNIST dataset during training.

	SVHN Alea.	SVHN Epist.	CelebA Alea.	CelebA Epist.	OODom Alea.	OODom Epist.
Dropout	84.67 \pm 1.42	75.79 \pm 0.86	75.95 \pm 3.61	75.00 \pm 3.21	21.75 \pm 6.36	78.81 \pm 6.91
Ensemble	88.08 \pm 0.85	85.70 \pm 0.70	78.80 \pm 0.82	77.63 \pm 0.61	40.53 \pm 9.95	96.71 \pm 2.31
NatPE	89.52 \pm 0.30	*87.31 \pm 1.47	*80.44 \pm 0.85	*83.46 \pm 2.40	93.16 \pm 2.11	98.99 \pm 0.64
R-PriorNet	99.94 \pm 0.01	99.98 \pm 0.00	74.69 \pm 2.39	70.63 \pm 6.14	64.45 \pm 10.72	59.61 \pm 13.23
EnD²	*89.56 \pm 0.67	84.36 \pm 0.84	77.94 \pm 1.62	78.14 \pm 1.66	53.05 \pm 6.07	4.42 \pm 2.57
PostNet	85.52 \pm 0.58	84.25 \pm 0.90	75.68 \pm 2.05	77.96 \pm 2.05	93.00 \pm 2.46	97.22 \pm 0.86
NatPN	86.37 \pm 1.27	83.18 \pm 1.49	77.44 \pm 1.48	79.43 \pm 2.29	*98.68 \pm 0.78	*99.78 \pm 0.12

Table 17: CIFAR-10 - OOD detection with AUC-ROC scores. Bold numbers indicate best score among single-pass models. Starred numbers indicate best scores among all models. Gray numbers indicate that R-PriorNet has seen samples from the SVHN dataset during training.

	Winter Epist.	Spring Epist.	Autumn Epist.	OODom Epist.
Dropout	53.98 \pm 1.60	51.24 \pm 0.96	53.89 \pm 1.16	*100.00 \pm 0.00
Ensemble	*81.53 \pm 1.11	*67.07 \pm 0.55	67.78 \pm 1.31	*100.00 \pm 0.00
EvReg	55.26 \pm 2.14	53.76 \pm 1.35	52.39 \pm 1.31	47.68 \pm 17.67
NatPN	78.99 \pm 4.07	63.61 \pm 4.00	*69.40 \pm 3.01	*100.00 \pm 0.00

Table 18: Bike Sharing (Normal \mathcal{N}) - OOD detection with AUC-ROC scores. Bold numbers indicate best score among single-pass models. Starred numbers indicate best scores among all models.

	Winter Epist.	Spring Epist.	Autumn Epist.	Winter OODom Epist.
Dropout	55.30 \pm 0.58	50.75 \pm 0.56	59.05 \pm 1.15	*100.00 \pm 0.00
Ensemble	95.31 \pm 0.41	75.62 \pm 0.85	78.93 \pm 1.35	*100.00 \pm 0.00
NatPN	*96.46 \pm 1.25	*77.73 \pm 2.74	*79.71 \pm 3.59	*100.00 \pm 0.00

Table 19: Bike Sharing (Poisson Poi) - OOD detection with AUC-ROC scores. Bold numbers indicate best score among single-pass models. Starred numbers indicate best scores among all models.